Review | Open Access

Energy Z

Li *et al. Energy Z* **2026**, *2*, 200024 **DOI:**10.20517/energyz.2026.39

Review of GeTe thermoelectric materials: recent progress, challenges and prospects

Song Li, Yang Geng, Hang Xu, Qi Zhang, Guodong Tang*

Keywords:
GeTe thermoelectrics, electrical transport optimization, phase transition, lattice thermal conductivity suppression, thermoelectric devices

Citation: Li, S.; Geng, Y.; Xu, H.; Zhang, Q.; Tang, G. Review of GeTe thermoelectric materials: recent progress, challenges and prospects. *Energy Z* **2026**, *2*, 200024. https://dx.doi.org/10.20517/energyz.2026.39

Received: 15 Sep 2026 **First Decision:** 30 Sep 2026 **Revised:** 19 Oct 2026 **Accepted:** 10 Nov 2026 **Published:** 26 Nov 2026

Academic Editor: Yuping Wu **Copy Editor:** Shu-Yuan Duan **Production Editor:** Shu-Yuan Duan

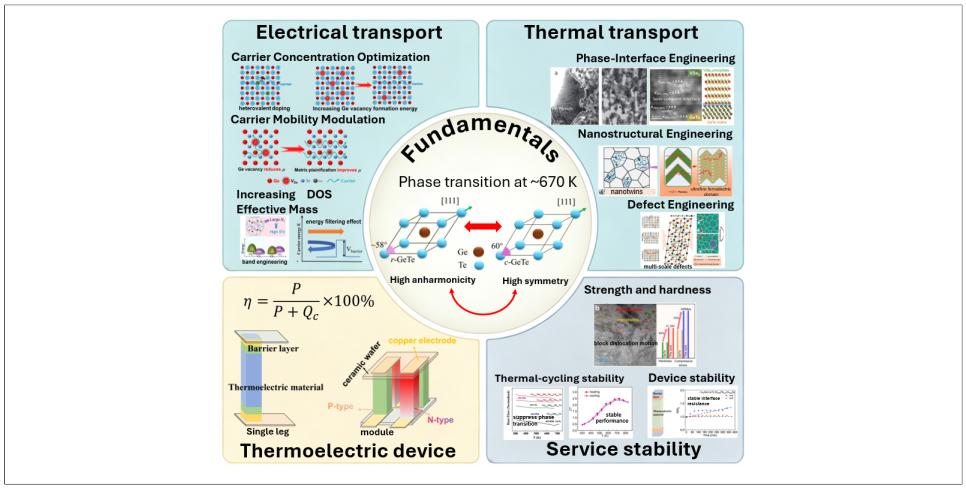

Abstract

Germanium telluride (GeTe) is a promising lead-free thermoelectric material for intermediate-temperature power generation because of its intrinsically favorable electronic structure and strong anharmonicity. However, its performance is limited by excessive hole concentrations associated with Ge vacancies, the temperature-dependent rhombohedral-to-cubic phase transition, and the trade-off between electrical and thermal transport. This review summarizes recent advances in GeTe-based thermoelectrics from the perspectives of carrier modulation, electronic-band engineering, phonon transport engineering, device fabrication, and service reliability, with dedicated sections on n-type GeTe and thin films. We first discuss the structural, electronic, and phononic origins of the thermoelectric properties of GeTe. We then compare strategies for optimizing carrier concentration and carrier mobility and for enhancing the density-of-states effective mass. We analyze approaches to suppressing lattice thermal conductivity through defect engineering, phase-interface engineering, and nanostructural engineering. Moreover, particular attention is given to improving the conversion efficiency of GeTe thermoelectric devices and to service reliability. Finally, we discuss the remaining challenges, including coupled electron-phonon optimization, long-term service stability, n-type GeTe optimization, and highly efficient thermoelectric devices. This review aims to provide guidance for optimizing the material properties, enhancing the mechanical reliability, and advancing device-level applications of

Check for updates

School of Materials Science and Engineering, Nanjing University of Science and Technology, Nanjing 210094, Jiangsu, China.

***Correspondence to:** Prof. Guodong Tang, School of Materials Science and Engineering, Nanjing University of Science and Technology, Nanjing 210094, Jiangsu, China. E-mail: tangguodong@njust.edu.cn

GeTe materials, thereby promoting the commercialization of GeTe thermoelectric materials.

INTRODUCTION

The escalating global energy crisis and environmental concerns have intensified the demand for sustainable energy conversion technologies[1]. Thermoelectric materials, which directly convert waste heat into electricity via the Seebeck effect, offer unique advantages (no moving parts, silent operation, and long service life), making them attractive for applications ranging from automotive exhaust recovery and industrial waste-heat utilization to deep-space power generation[2]. The conversion efficiency of a thermoelectric material is governed by the dimensionless figure of merit, $ZT = S^2\sigma T/\kappa_T$, where S, σ, κ_T, and T are the Seebeck coefficient, electrical conductivity, thermal conductivity, and absolute temperature, respectively. The total thermal conductivity (κ_T) comprises electronic (κ_e) and lattice (κ_L) contributions, while the power factor ($PF = S^2\sigma$) serves as a measure of electrical transport performance[3]. Achieving high ZT requires maximizing the power factor while minimizing thermal conductivity, which is a great challenge due to the strong interdependence of S, σ, and the electronic contribution to κ_e [4].

Among various thermoelectric systems, GeTe has emerged as one of the most promising lead-free candidates for mid-temperature (500-800 K) power generation[5]. Compared with PbTe-based counterparts, GeTe provides competitive thermoelectric performance in a lead-free and more environmentally friendly composition[6]. Its exceptional electronic band structure, featuring multiple valence bands with small effective mass and high valley degeneracy, provides a good foundation for high power factors[7]. Nevertheless, pristine GeTe suffers from intrinsically high hole concentrations (~ 10^{21} cm^{-3}) arising from low-formation-energy Ge vacancies, which severely limit its performance[8]. Additionally, the rhombohedral-to-cubic phase transition at ~ 670 K, while beneficial for band degeneracy, poses device-stability challenges due to thermal expansion mismatch and internal stress[9].

Significant progress in ZT enhancement has been achieved over the past decade[10,11]. The peak ZT and average ZT have generally improved continuously over the past ten years, as shown in Figure 1A and B. A record-high ZT of ~ 2.7 was achieved in the $Ge_{0.94}Bi_{0.05}Te$-0.1 wt.% TiB_2 sample, whereas an average ZT of ~ 1.9 was achieved in the $(Ge_{0.82}Mn_{0.04}Bi_{0.04}Pb_{0.1}Te)_{0.99}(VSe_2)_{0.01}$ sample[10,12]. Substantial efforts have been devoted to overcoming these limitations through carrier concentration optimization, band engineering, and multiscale defect engineering[13]. A comprehensive review integrating recent mechanistic studies and advances in GeTe property optimization, mechanical performance, and device conversion efficiency is still lacking. This review aims to fill this gap by providing a critical and systematic overview of recent progress in GeTe-based thermoelectrics and devices. We begin by discussing the fundamental crystal structure, phase transition, and band characteristics. We then critically evaluate strategies for optimizing electrical transport, including carrier concentration optimization, carrier mobility enhancement, and density-of-states (DOS) effective mass enhancement. Subsequently, we examine thermal transport suppression through defect engineering, phase-interface engineering, and nanostructural engineering. We also address device-level performance and service reliability, highlighting recent record conversion efficiencies. We further discuss recent progress in n-type GeTe and GeTe-based thin films. Finally, we identify remaining challenges and outline future research directions, with an emphasis on balanced electron-phonon optimization and practical device integration.

This review emphasizes the synergistic optimization of electronic and thermal transport, with particular attention to phase-transition manipulation and the translation of material-level ZT into device-level efficiency[14-16]. Moreover, this review treats service reliability as a dedicated topic, covering phase-transition-related thermal-expansion mismatch and cracking, mechanical strengthening, and thermal-cycling

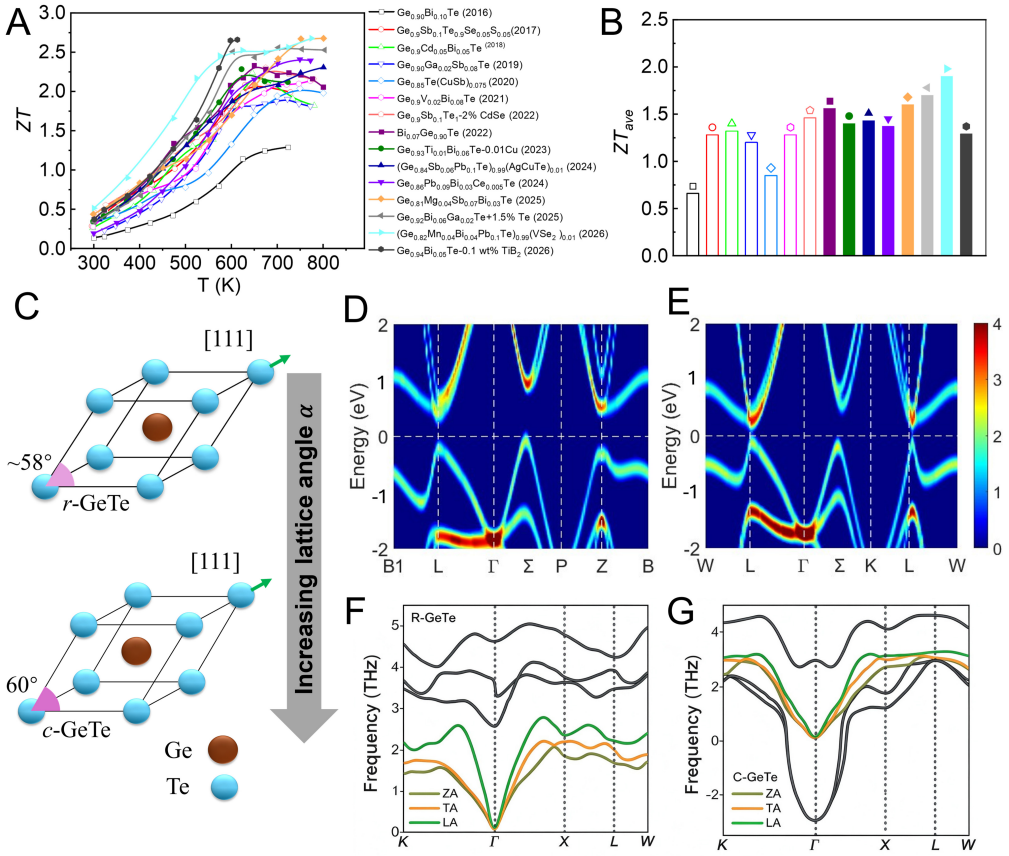

Figure 1. (A) Temperature-dependent *ZT* and (B) average *ZT* (ZT_{avg}) of representative GeTe-based materials, illustrating the progress made in this field over the past decade[6,10,12,62,79,92,99,103,105,119,143,164-167]; (C) Primitive cells of rhombohedral *r*-GeTe and cubic *c*-GeTe along the [111] direction; (D) Calculated band structure of *r*-GeTe; (E) calculated band structure of *c*-GeTe; (F) Phonon dispersion of *r*-GeTe; and (G) phonon dispersion of *c*-GeTe. Figure 1F and G is adapted from Ref.[17] with permission. Copyright © 2020 Wiley. *ZT*: Dimensionless figure of merit.

stability-topics addressed only briefly in previous reviews of GeTe. This review also covers recent advances in the field of GeTe, including contributions from our research group. By systematically summarizing the relevant optimization strategies and underlying mechanisms, we aim to provide a framework for balanced electron-phonon co-optimization that extends from fundamentals to device applications.

FUNDAMENTALS

Crystal structure

GeTe exists in two polymorphic phases [Figure 1C]: a low-temperature rhombohedral phase (*r*-GeTe, space group *R3m*) and a high-temperature cubic phase (*c*-GeTe, space group *Fm3m*)[17]. The rhombohedral phase can be described by a hexagonal unit cell with lattice parameters a = b = 4.156 Å and c = 10.663 Å, while the cubic phase possesses a rock salt structure with a = 6.01 Å[17]. The formation of the rhombohedral phase is driven by a Peierls distortion, which originates from the hybridization between the Ge $4s^2$ lone-pair electrons and the Te p orbitals[18]. This hybridization lowers the system energy by driving the Ge cations to displace off-center along the [111] direction, resulting in a distorted rhombohedral structure with alternating short and long Ge-Te bonds[19].

Upon heating, enhanced atomic thermal vibrations weaken this resonant bonding, rendering the Peierls distortion unsustainable[20]. The rhombohedral-to-cubic transition temperature of GeTe is commonly reported in the range of approximately 650-700 K, depending on composition, Ge-vacancy concentration,

doping level, and measurement method[21]. During this transition, the Ge atoms shift from the off-center position (0.5-x, 0.5-x, 0.5-x) in the rhombohedral lattice to the body-center position (0.5, 0.5, 0.5) in the cubic lattice. As a result, the six Ge-Te bonds become equal in length, and the lattice relaxes to the high-symmetry cubic structure[22]. Neutron and synchrotron diffraction reveal that this evolution involves continuous changes in the rhombohedral angle and Ge displacement, rather than a discrete two-state transition[23]. Notably, an anomalous volume contraction near the transition[24], combined with abrupt thermal expansion changes, generates internal stress and increases the risk of cracking in devices[25].

Energy band and phonon spectrum

r-GeTe and *c*-GeTe exhibit distinct band structures arising from their different crystal symmetries[26]. The calculated Fermi surface and the band structure of GeTe materials in the rhombohedral and cubic phases are shown in Figure 1D and E, respectively. According to density functional theory (DFT) calculations, GeTe is a narrow-band-gap semiconductor with an indirect band gap of approximately 0.56 eV (*r*-GeTe) and a direct band gap of approximately 0.37 eV (*c*-GeTe)[17,27]. Orbital-projected density of states (DOS) analysis indicates that contributions from the Ge-4s and Te-5p orbitals to the valence-band edge, together with the strength of local s-p bonding, determine the energy difference (ΔE)[28]. The valence band edges of *r*-GeTe are located at the L, Σ, and Z points, respectively. The calculated energy difference between L and Σ ($E_{\Sigma\text{-L}}$) is 0.15 eV; that between Σ and Z ($E_{\Sigma\text{-Z}}$) is 0.20 eV[7,29]. In high-symmetry *c*-GeTe, the small energy difference between the L and Σ bands in the pristine material contributes to a high valley degeneracy of 16[30]. Compared with those of SnTe and PbTe, the band structure of GeTe features a small effective mass and high valley degeneracy, thereby supporting favorable intrinsic electrical transport[17]. The outstanding band structure gives GeTe materials good potential for electrical property modulation.

The phonon spectrum of GeTe [Figure 1F and G] is governed by strong anharmonicity originating from the stereochemically active Ge $4s^2$ lone pairs, which gives rise to large Grüneisen parameters, low phonon group velocities, and intense phonon-phonon (umklapp) scattering[31,32]. Inelastic scattering experiments and first-principles calculations show that the optical phonon branches are anomalously low-lying and strongly overlap with the acoustic branches; the resulting acoustic-optical coupling further flattens the acoustic dispersion and suppresses the phonon group velocity[33,34]. However, the intrinsic anharmonicity alone is insufficient: pristine GeTe still exhibits a lattice thermal conductivity of ~ 1.6 W m^{-1} K^{-1} at room temperature, which must be further suppressed for high *ZT*. Since both the soft polar mode and the lone-pair-driven anharmonicity are highly tunable, doping and alloying that modify the polar distortion or the chemical bonding provide effective routes to reduce the lattice thermal conductivity[32,35].

Phase transition: a double-edged sword

The rhombohedral-to-cubic phase transition of GeTe acts as a double-edged sword in thermoelectric applications. On the one hand, the transition is closely linked to the superior band structure of cubic GeTe, which yields a high valley degeneracy of up to 16 and hence a large DOS effective mass and power factor[17,30]. Extending the high-symmetry cubic structure to lower temperatures by suppressing or shifting the transition via doping and alloying further promotes valence-band convergence and enhances the Seebeck coefficient[36-38]. On the other hand, the transition occurs at ~ 670 K, right within the target operating window (500-800 K) of GeTe-based power generation. The phase transition can adversely affect the reliability of both the material and the devices. This transition involves an anomalous volume contraction of approximately 0.6% and an abrupt change in the coefficient of thermal expansion[24]. Consequently, internal stresses are generated each time the material is heated or cooled through the transition temperature. These stresses cause microcracking, interfacial delamination, and solder failure, threatening the mechanical integrity and long-term reliability of devices[24,39,40]. Accordingly, engineering the phase transition by suppressing or shifting it while preserving the favorable high-symmetry band structure is a central concern in optimizing GeTe thermoelectric performance[41].

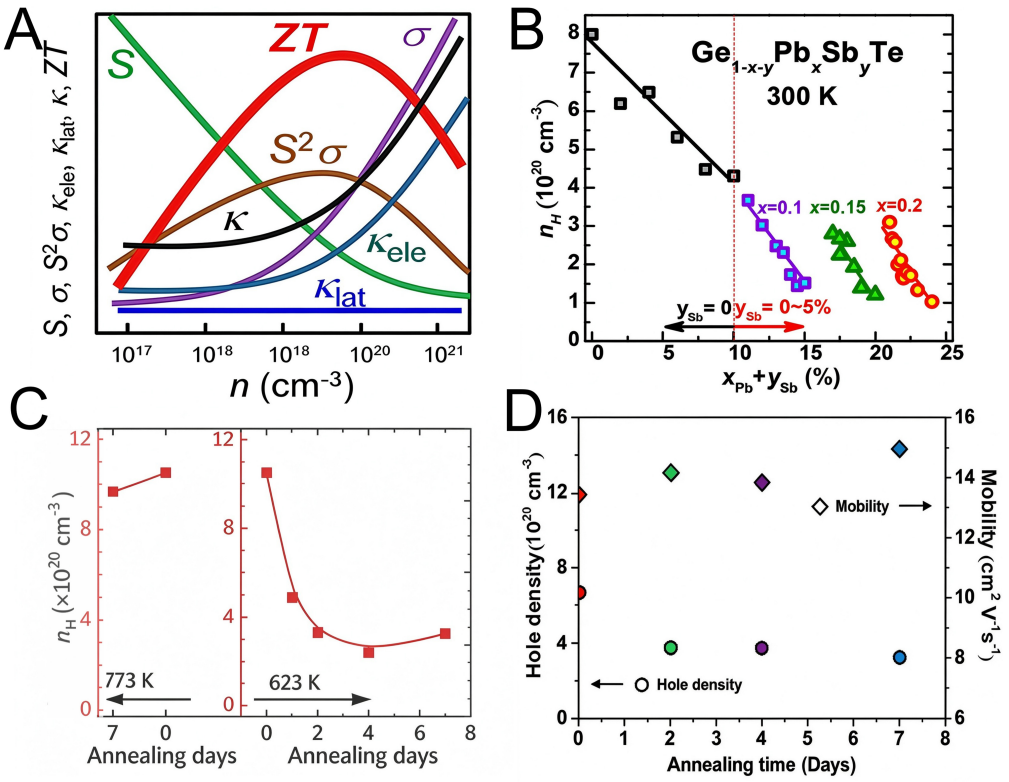

Figure 2. (A) Relationship between thermoelectric parameters and carrier concentration. Figure 2A is adapted from Ref.[45] with permission. Copyright © 2016 American Chemical Society; (B) Composition-dependent carrier concentration for $Ge_{1-x-y}Pb_xSb_yTe$ at room temperature. The different symbols denote samples with different Pb and Sb contents: black squares, y_{Sb} = 0 (x_{Pb} = 0-0.10); purple squares, x_{Pb} = 0.10 (y_{Sb} = 0-0.05); green triangles, x_{Pb} = 0.15 (y_{Sb} = 0-0.05); red circles, x_{Pb} = 0.20 (y_{Sb} = 0-0.05). Figure 2B is adapted from Ref.[38] with permission. Copyright © 2018 American Chemical Society; (C) Evolution of *n* for GeTe samples annealed at 773 and 623 K, respectively. Figure 2C is adapted from Ref.[46] with permission. Copyright © 2023 Wiley; (D) Annealing time dependence of hole density and mobility. Figure 2D is adapted from Ref.[61] under the CC BY 4.0 license. *ZT*: Dimensionless figure of merit.

ENHANCING ELECTRONIC TRANSPORT

Carrier concentration optimization

Pristine GeTe exhibits p-type conductivity because the low formation energy of Ge vacancies generates a high concentration of vacancies in the matrix[42], thereby yielding the high intrinsic carrier concentration of ~ 10^{21} cm^{-3}. Under the single-parabolic-band (SPB) approximation, the Seebeck coefficient is determined by the reduced Fermi level, the DOS effective mass, and the dominant carrier-scattering mechanism. The Seebeck coefficient of the GeTe system can be simplified by assuming an acoustic-phonon scattering mechanism with a scattering parameter of r = -1/2, as follows[43]:

$$S = \frac{8\pi^2 k_B^2 T}{3eh^2} m_d^* \left(\frac{\pi}{3n}\right)^{\frac{2}{3}} \quad (1)$$

where k_B is the Boltzmann constant, h is the Planck constant, m_d^* is the DOS effective mass, and n is the carrier concentration. However, in heavily doped GeTe, ionized-impurity scattering (r = +3/2) and alloy-disorder scattering are comparable to or even dominant over acoustic-phonon scattering. The simplified expression is therefore reliable only as a qualitative guide to the inverse *S*-*n* correlation. Figure 2A shows that the Seebeck coefficient is inversely proportional to the carrier concentration; therefore, the excessively high carrier concentration severely limits the thermoelectric performance and further practical applications of GeTe[44,45]. The optimal carrier concentration for GeTe is in the range of 1 ~ 3 × 10^{20} cm^{-3}[46]. To meet this requirement, strategies involving charge compensation and carrier-concentration engineering have been proposed.

Several strategies have been developed to optimize the carrier concentration of GeTe. One common approach is heterovalent doping (e.g., Bi^{3+}[47], Sb^{3+}[41], Fe^{3+}[48], Sc^{3+}[49], I^{1-}[50,51]), which compensates excessive holes and reduces carrier density to the desired range. For instance, Bi substitution at the Ge site provides one more electron than Ge^{2+}, effectively counteracting the excessively high hole concentration induced by intrinsic Ge vacancies, thereby achieving a peak *ZT* of ~ 2.0[47]. Sb doping can similarly optimize the carrier concentration while also increasing crystal symmetry[52].

Another strategy involves introducing dopants such as Cu[53,54], Pb[38,55], and Ca[56] to increase the formation energy of Ge vacancies, thereby lowering carrier concentration. This approach is particularly attractive because it suppresses the formation of Ge vacancies at the source to address the excessively high carrier concentration, rather than merely compensating for them[57]. For instance, Pb doping increases the formation energy of Ge vacancies by increasing the cation-to-anion size ratio. As the Pb content increases [Figure 2B], the formation of Ge precipitates is suppressed, reducing the intrinsic hole concentration to the optimal range (~ 10^{20} cm^{-3}) and synergistically improving the electrical transport properties[38,58].

Beyond chemical doping, process optimization has also proven effective in raising the vacancy formation energy[59]. By tailoring the preparation and heat-treatment process, the microstructure and defects of the material can be effectively modulated. Theoretical calculations indicate that lattice strain can efficiently elevate the formation energy of Ge vacancies, and that introducing substantial lattice distortion into the GeTe matrix is expected to hinder the formation of Ge vacancies[60]. Liu *et al.* employed a non-equilibrium preparation route (high-energy ball milling combined with spark plasma sintering) to introduce lattice strain, which was shown to efficiently suppress vacancy formation and reduce carrier concentration[60]. Annealing can also reduce the carrier concentration in GeTe. Zhang *et al.* proposed annealing below the phase transition temperature at 623 K. Due to the higher formation energy of Ge vacancies in the rhombohedral phase[8], this annealing allows Ge atoms to migrate and fill the vacancies, reducing the carrier concentration from ~ 10.5 × 10^{20} cm^{-3} to ~ 3 × 10^{20} cm^{-3} [Figure 2C][46]. Extended heat-treatment periods can also effectively modulate the type and distribution of intrinsic point defects. Xu *et al.* demonstrated that seven days of annealing promoted the migration and recombination of Ge vacancies into long-range gaps in pseudo-layered $Sb_2Te_3(GeTe)_{17}$, effectively lowering the hole carrier concentration in Figure 2D[61].

Collectively, these studies demonstrate that carrier concentration optimization, whether through aliovalent doping, vacancy formation energy enhancement, or post-synthesis processing, constitutes the essential first step toward high *ZT* in GeTe.

Carrier mobility modulation

While optimizing the carrier concentration is the first step toward improving *ZT*, it is equally important to maintain or even enhance carrier mobility. The electrical conductivity of a material is directly related to its carrier concentration and mobility via the relation $\sigma = ne$, in which n and denote the carrier concentration and mobility, respectively, and e is the elementary charge[14]. Although increasing carrier concentration can enhance electrical conductivity, an excessively high carrier concentration severely deteriorates the Seebeck coefficient in the GeTe system. Carrier mobility plays a pivotal role in determining the electrical transport performance of thermoelectric materials, as it directly governs the electrical conductivity for a given carrier concentration. Improving carrier mobility means further enhancing electrical conductivity and power factor without compromising the Seebeck coefficient. In GeTe, intrinsic Ge vacancies cause excessive hole concentrations and severe carrier scattering, leading to low mobility[62].

The carrier mobility can be expressed as $\mu \propto \cdot m_b^{*-5/2}$ for acoustic phonon scattering, where m_b^* is the band effective mass[63]. The band effective mass is inversely proportional to the band curvature, meaning that a larger band curvature corresponds to a lower band effective mass and, consequently, a higher carrier

mobility[64]. This means that if band sharpening can be facilitated, the mobility can be enhanced. Y doping was initially found to be effective in enhancing the carrier mobility of GeTe. Gao *et al.* reported that Y substitution significantly increased the Hall mobility from ~ 17 $cm^2 V^{-1} s^{-1}$ in pristine GeTe to ~ 35 $cm^2 V^{-1} s^{-1}$ in $Ge_{0.98}Y_{0.02}Te$ at room temperature[65]. Subsequently, Liu *et al.* provided a deeper mechanistic understanding through first-principles calculations, revealing that Y doping sharpens the valence band maximum (VBM)[66]. The valence-band maximum of GeTe is dominated by the Ge-4s and Te-5p orbitals, and the dispersion of the VBM is governed by orbital interaction within the Ge-Te-Ge bonding network[32]. Y substitutes at the Ge site as a trivalent cation. Its higher-lying Y-4d states interact with the Ge-Te antibonding states at high energies, which enhances the charge transfer from the cation to Te (from 0.19 e in pristine GeTe to 0.23 e in Y-doped GeTe)[66]. This enhanced charge transfer strengthens the contribution of the Ge-4s electrons to the valence band, so that the VBM becomes more dispersive, which is the physical origin of band sharpening. This band sharpening increases the energy separation between light and heavy valence bands (ΔE from 0.08 to 0.13 eV), which effectively suppresses interband scattering and substantially improves carrier mobility from ~ 81 to ~ 159 $cm^2 V^{-1} s^{-1}$ at 300 K[66].

The lattice plainification strategy can increase carrier mobility by weakening carrier scattering from lattice defects[67,68]. Recent studies, illustrated in Figure 3A, demonstrate that Cu doping can effectively plainify the GeTe lattice by filling Ge vacancies. This strategy effectively suppresses vacancy scattering and substantially improves carrier mobility [Figure 3B][42,54]. Beyond atomic filling, increasing the formation energy of Ge vacancies offers an alternative route to reduce vacancy scattering and improve mobility[5,69,70]. This approach is particularly attractive because it simultaneously lowers the carrier concentration, realizing both concentration optimization and scattering suppression[46,59,61]. For example, Zhang *et al.* [Figure 3C] demonstrated that annealing rhombohedral GeTe below the phase transition temperature effectively suppresses excessive vacancies, which not only reduces the hole concentration but also weakens vacancy scattering, leading to a record-high mobility of ~ 150 $cm^2 V^{-1} s^{-1}$ at 300 K, far exceeding that of conventional counter-doped GeTe (≤ 60 $cm^2 V^{-1} s^{-1}$)[46].

In addition to band sharpening and lattice plainification, alternative strategies have been developed to enhance carrier mobility. When excess Cu is added to GeTe, Cu atoms can occupy interstitial sites in the matrix, altering the charge distribution between Ge and Te atoms and providing an additional channel for carrier transport that weakens carrier scattering[62]. In addition to the transport channels provided by interstitial Cu, reducing the equivalent deformation potential through interfacial constraint can directly suppress carrier scattering[10]. Yu *et al.* combined the $Ge_{0.94}Bi_{0.05}Te$ matrix with high-modulus TiB_2 nanoparticles. The induced interfacial constraint effect increases the longitudinal elastic modulus and decreases the equivalent deformation potential, thereby improving carrier mobility[10]. Besides, growing high-quality GeTe single crystals directly enhances carrier mobility by removing grain-boundary scattering, the dominant extrinsic scattering source in polycrystalline GeTe[71]. High-quality Sb-doped single crystals achieve a record power factor of ~ 56 W $cm^{-1} K^{-2}$ and ZT 2.2[72].

Increasing DOS effective mass

A large DOS effective mass (m_d^*) is essential for achieving a high Seebeck coefficient (S), because S is proportional to m_d^*. m_d^* is defined as $m_d^* = N_v^{2/3} m_b^*$, where N_v is the band degeneracy (number of valleys or pockets) and m_b^* is the single-band effective mass[73]. This relationship highlights that m_d^* can be increased either by enlarging the single-band mass or by enhancing the valley degeneracy through band convergence or crystal-symmetry modification in GeTe thermoelectric materials.

Figure 4A schematically shows that enhancing the valley degeneracy by band convergence and band alignment is an effective strategy for GeTe. Previous studies have demonstrated that doping with elements such as Mg[74], Ca[2,75], Zn[76,77], Hg[78], Cd[79], and I[80] can reduce the energy offset (ΔE) between the light (L)

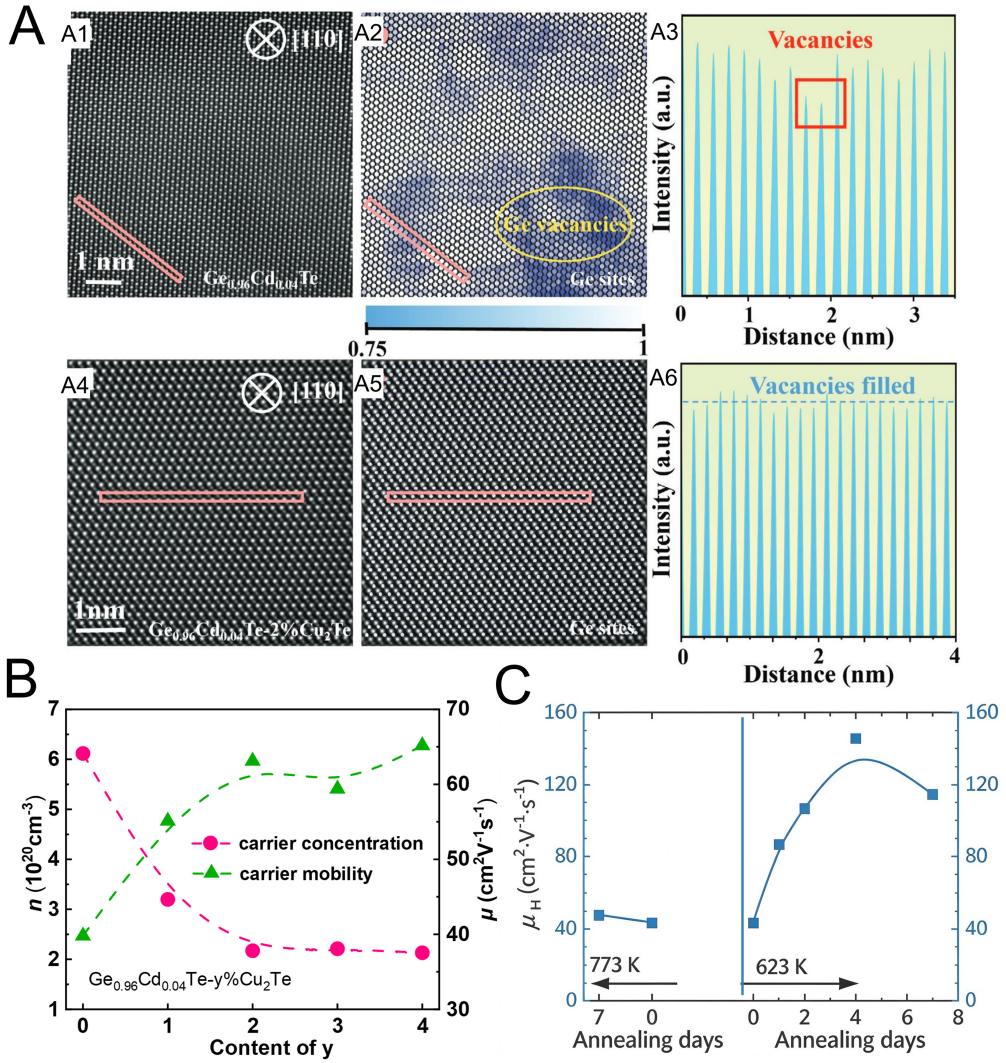

Figure 3. (A) Comparison of the microstructure of $Ge_{0.96}Cd_{0.04}Te$ and $Ge_{0.96}Cd_{0.04}Te$-2%Cu_2Te samples at the atomic scale, showing that the Ge vacancies are filled with Cu atoms; (B) Evolution of n and μ for $Ge_{0.96}Cd_{0.04}Te$-y%Cu_2Te samples. Figure 3A and B is adapted from Ref.[42] under the CC BY 4.0 license; (C) Evolution of μ for GeTe samples annealed at 773 and 623 K, respectively. Figure 3C is adapted from Ref.[46] with permission. Copyright © 2023 Wiley.

and heavy (Σ) valence bands, thereby promoting the participation of the heavy band in electrical transport and realizing band convergence [Figure 4B and C]. However, these approaches typically yield a valley degeneracy in the range of 4-16, as they only consider the L and Σ bands, while the third valence band is often neglected. Achieving convergence of all three valence bands can further increase the valley degeneracy. Hong *et al.* demonstrated that Cr doping induces the convergence of three valence band edges in both rhombohedral and cubic GeTe[81]. Consequently, convergence of the three bands effectively improves the power factor across the entire temperature range[81]. Furthermore, the alignment of the three valence bands is successfully achieved in $CuBiS_2$-alloyed GeTe [Figure 4D and E]. Li *et al.* attained an ultrahigh valley degeneracy (N_v) of 22 in $CuBiS_2$-alloyed GeTe[82]. $CuBiS_2$ alloying in GeTe induces a refined valence band alignment among the three valence band maxima (VBM1 at the L point with N_v = 4, VBM2 at the Σ point with N_v = 12, and VBM3 along the Γ-X direction with N_v = 6)[82]. Density functional theory calculations reveal that $CuBiS_2$ alloying shifts the valence band maximum from the L point to the Σ point and significantly reduces the energy offsets between the three bands: $\Delta E^{(VBM1\text{-}VBM2)}$ decreases from 67 meV to -16 meV, and $\Delta E^{(VBM1\text{-}VBM3)}$ decreases from 273 meV to 63 meV[82]. This band alignment among all three valence bands yields

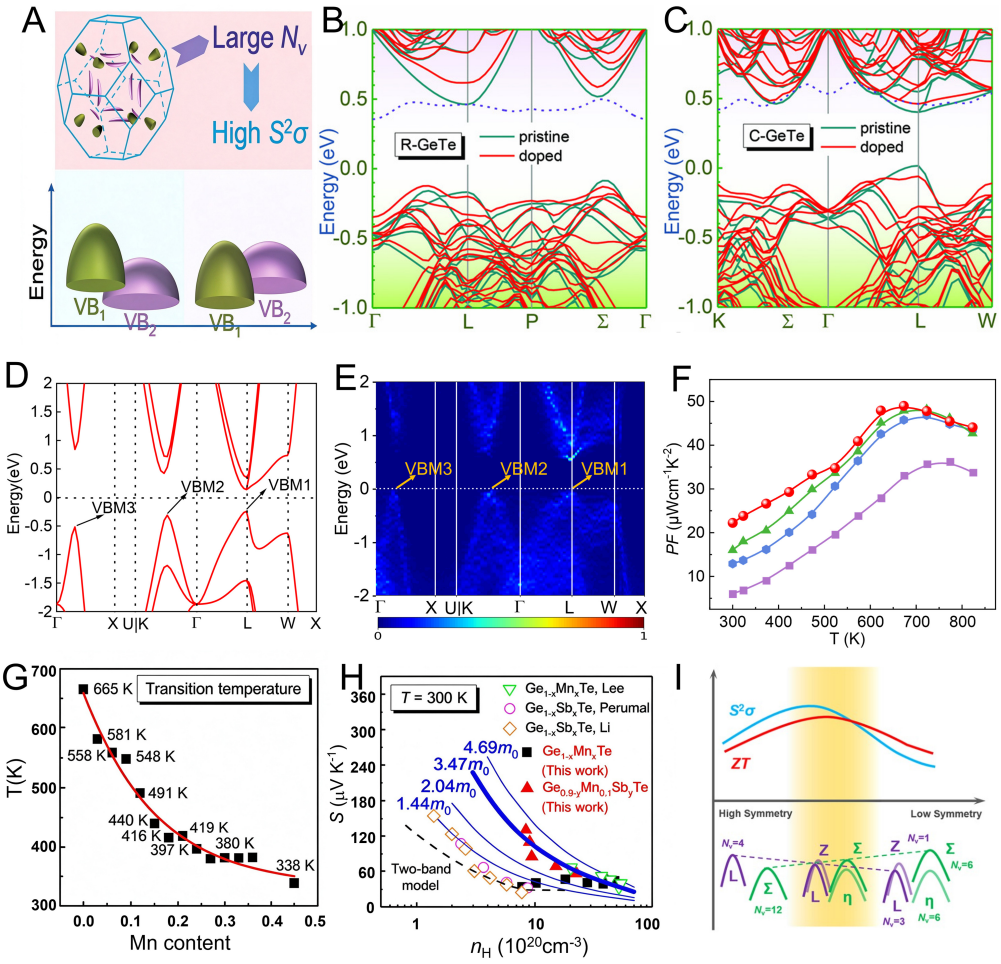

Figure 4. (A) Schematic illustration of enhanced band degeneracy; Figure 4A is adapted from Ref.[76] with permission. Copyright © 2019 American Chemical Society; (B) Calculated band structures for pure and Cd-doped GeTe in the rhombohedral phase. (C) Calculated band structures for pure and Cd-doped GeTe in the cubic phase. Figure 4B and C is adapted from Ref.[79] with permission. Copyright © 2018 Wiley; (D) calculated electronic band structure of pristine GeTe; (E) Calculated electronic band structure of $Ge_{63}Cu_6Bi_6Te_{63}S_{12}$; (F) Power factor (*PF*) of $(GeTe)_{1-x}(CuBiS_2)_x$ samples. Figure 4D-F is adapted from Ref.[82] under the CC BY 4.0 license; (G) Transition temperatures as a function of Mn content in $Ge_{1-x}Mn_xTe$ obtained from differential scanning calorimetry (DSC) curves; (H) Pisarenko plot for $Ge_{1-x}Mn_xTe$ compounds compared with previously reported results. Figure 4G and H is adapted from Ref.[88] with permission. Copyright © 2018 American Chemical Society; (I) Schematic illustration of symmetry reduction and its effect on band degeneracy. Figure 4I is adapted from Ref.[38] with permission. Copyright © 2018 American Chemical Society. VBM: Valence band maximum; N_v: valley degeneracy; *ZT*: figure of merit.

an ultra-high total valley degeneracy of $N_v = 4 + 12 + 6 = 22$. The ultra-high valley degeneracy dramatically enhances the DOS effective mass (m_d^* increases from 1.03 m_0 for pristine GeTe to 2.23 m_0 for the optimal composition), leading to a substantially enhanced Seebeck coefficient and power factor across the entire temperature range [Figure 4F].

Besides enhancing the valley degeneracy, the DOS effective mass can also be enlarged by increasing the band effective mass through band flattening. Because the band effective mass is inversely proportional to the band curvature, flattening the band dispersion enlarges m_b^* and therefore $m_d^* = N_v^{2/3} m_b^*$, which enhances the Seebeck coefficient. The band-flattening effect has been reported in $AgBiSe_2$-alloyed GeTe and Ca-Sb co-doped GeTe[2,83]. Together with band convergence, it increases the DOS near the Fermi level and thus the DOS effective mass, thereby improving the Seebeck coefficient and power factor. Band flattening and band convergence are therefore complementary, since they increase m_d^* through its two independent factors, m_b^*

N_v, respectively. Nevertheless, band flattening has its downside: the increase in m_b^* that raises the Seebeck coefficient also reduces the carrier mobility $\mu \propto \cdot m_b^{*-5/2}$ under acoustic-phonon scattering, so that excessive band flattening can degrade the power factor. Moreover, a flattened band contributes to transport only when it lies sufficiently close to the Fermi level[2].

Manipulating the crystal symmetry of GeTe is a powerful strategy to optimize the electronic band structure and achieve high thermoelectric performance. The phase transition point between rhombohedral and cubic GeTe is at ~ 670 K, with the rhombohedral phase approximated as a directionally distorted cubic lattice along the [111] direction. This distortion from *c*-GeTe to *r*-GeTe splits the original 4L valleys into 3L + 1Z valleys and the 12Σ valleys into 6Σ + 6η valleys, while also reversing the energy ordering of the L and Σ bands[84]. The degree of rhombohedral distortion (quantified by the rhombohedral angle) can be continuously tuned via doping and alloying[85]. Studies have shown that Ti[86], Mn[87,88], and Sb[89] doping can effectively manipulate the crystal symmetry of GeTe. In particular, Zheng *et al.* demonstrated that increasing the Mn content drives the crystal structure from the rhombohedral toward the high-symmetry cubic phase and high Mn doping even stabilizes the cubic phase at room temperature [Figure 4G][88]. This symmetry enhancement successfully extends the high valley degeneracy characteristic of the cubic phase to the low-temperature range, while simultaneously promoting valence band convergence by decreasing the energy offset between the L and Σ bands, thereby effectively enhancing the DOS effective mass across the entire temperature range [Figure 4H][87,88]. Despite the general trend of increasing crystal symmetry, a slight reduction in symmetry can also increase N_v. Li *et al.* demonstrated that Sb doping not only optimizes carrier concentration but also controls the rhombohedral distortion by increasing the interaxial angle toward 90, effectively tuning the band structure[38]. As shown in Figure 4I, the Sb-induced distortion shifts the valence band maximum from the L point toward the Σ point, while splitting the L pockets into 3L + 1Z valleys and the Σ-related pockets into 6Σ + 6η valleys. The slight rhombohedral distortion minimizes the energy offsets (ΔE) between these bands, achieving a higher degeneracy (N_v = 16) than the fully cubic GeTe phase, resulting in a peak *ZT* of 2.4[38].

Introducing a resonant level can also increase the DOS effective mass of GeTe. It forms a weakly dispersed impurity band that hybridizes with the host valence band, causing a local distortion in the DOS near the Fermi level (E_f) without significantly altering the overall band structure[90,91]. For example, in Figure 5A, In doping introduces an In-p orbital impurity band within the band gap of GeTe that hybridizes with the valence band, creating a sharp DOS peak near E_f. As a result, the Seebeck coefficient (*S*) versus carrier concentration (*n*) data for In-Bi co-doped GeTe in Figure 5B shows the *S* and the DOS effective mass are greatly enhanced[91]. The introduction of In as a resonant energy level dopant further increases *S* from 155 V K^{-1} to 190 V K^{-1} at room temperature in the Sb-In co-doped GeTe. Consequently, the *PF* is substantially enhanced, with a maximum *PF* of ~ 38 W cm^{-1} K^{-2} achieved in $Ge_{0.89}Sb_{0.1}In_{0.01}Te$ [Figure 5C][36]. In addition to In, Ga also exhibits a resonant state in GeTe. DFT calculations in Figure 5D reveal that low-level Ga doping (< 2 mol%) introduces a sharp hump (resonant state) near the top of the valence band, characterized by a narrow plateau-like DOS and split-off bands from the VBM. This behavior resembles a resonant level effect, similar to that reported for In doping in GeTe, and arises from the interaction between Ga-4s and Te-5p, Ge-4s, and Ge-4p orbitals. However, unlike the In-induced state, the Ga-induced resonant state is not located at a favorable position near the Fermi level. Instead, Ga predominantly contributes to the top of the valence band, yet its induced DOS distortion in the matrix remains relatively modest[92,93]. In doping significantly enhances the Seebeck coefficient but simultaneously reduces carrier mobility and shrinks the band gap, leading to increased bipolar thermal conductivity at high temperatures. In contrast, Ga doping produces less severe mobility degradation and band-gap reduction. Liang *et al.* [Figure 5E] showed that co-doping In and Ga at a 1:1 ratio provides a compromise design that balances DOS enhancement, carrier mobility, and bipolar transport, achieving a peak *ZT* of 2.1 in $Ge_{0.78}In_{0.005}Ga_{0.005}Pb_{0.1}Sb_{0.07}Te$ [Figure 5F][94].

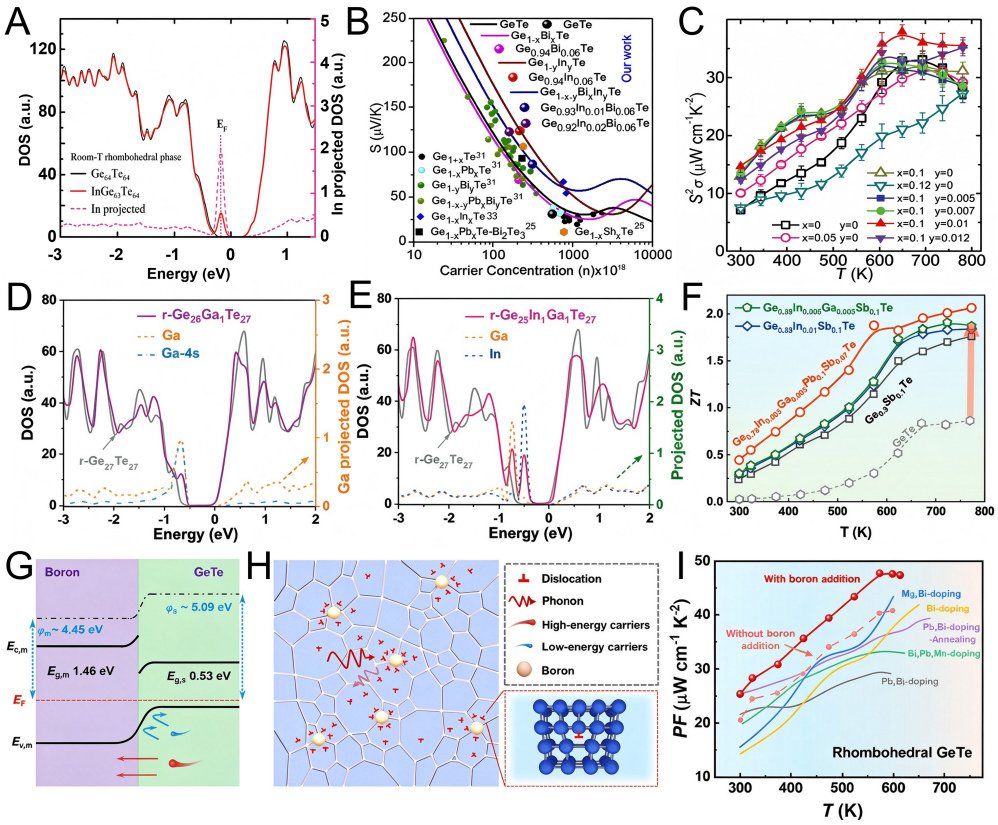

Figure 5. (A) Calculated DOS for $Ge_{64}Te_{64}$ and $In_1Ge_{63}Te_{64}$ in the room-temperature rhombohedral phase; (B) *S* versus *n* data for In-Bi co-doped GeTe and a comparison with previous reports. Figure 5A and B is adapted from Ref.[91] under the CC BY 4.0 license; (C) Temperature-dependent power factor of $Ge_{1-x-y}Sb_xIn_yTe$ samples. Figure 5C is adapted from Ref.[36] with permission. Copyright © 2018 Wiley; (D) total and projected DOS for *r*-$Ge_{26}Ga_1Te_{27}$; (E) Total and projected DOS for *r*-$Ge_{25}In_1Ga_1Te_{27}$; (F) Temperature-dependent *ZT* values illustrating the improvements achieved by progressively introducing Sb, In, Ga, and Pb into GeTe. Figure 5D-F is adapted from Ref.[94] with permission. Copyright © 2024 Wiley; (G) Schematic illustration of the energy-filtering effect; (H) Effects of boron/GeTe composites on carrier and phonon transport; (I) Temperature dependence of power factor for B/BGT samples (B0/BGT and B10/BGT samples) and comparison with other works. Figure 5G-I is adapted from Ref.[96] under the CC BY 4.0 license. DOS: Density of states; BGT: Bi-doped GeTe; *ZT*: figure of merit; *PF*: power factor; E_F: Fermi level.

The energy filtering effect is another strategy that can enhance the Seebeck coefficient. The energy filtering effect can arise from potential barriers at heterointerfaces between the GeTe matrix and secondary phases[95]. At these heterointerfaces, the energy level mismatch between the matrix and the secondary phases creates potential barriers that selectively scatter low-energy charge carriers while allowing high-energy carriers to pass, thereby increasing the average carrier energy and enhancing the Seebeck coefficient [Figure 5G][96]. This effect equivalently enhances the DOS effective mass without altering the intrinsic band structure. A significant energy filtering effect has been observed in GeTe composites incorporating CaTe[56], Fe_3O_4[97], MXene[98], and boron nanoparticles[96] as secondary phases. Notably, the heterogeneous interfaces constructed by incorporating boron nanoparticles into the GeTe matrix have proven effective in inducing the energy filtering effect [Figure 5H]. This approach increased the power factor to 25.4 W cm^{-1} K^{-2} at room temperature and to 47.7 W cm^{-1} K^{-2} at 573 K [Figure 5I].

Overall, the strategies discussed above, including heterovalent doping, vacancy engineering, band convergence, symmetry manipulation, resonant-level doping, and energy filtering, offer complementary routes to enhance the electronic transport of GeTe, yet each targets a specific bottleneck and inevitably interacts with others. For example, since doping tunes the carrier concentration but introduces extra scattering, it is important to balance the magnitude of a given beneficial mechanism, because an effect that is

helpful at a low level may become harmful when intensified. Also, the trade-off between the Seebeck coefficient and carrier mobility must be optimized by considering the weighted mobility[99], since any mechanism that increases the DOS effective mass also tends to reduce mobility. Importantly, rational multi-strategy integration, rather than single-parameter optimization, is therefore the key to further improving the electrical performance of GeTe thermoelectrics.

SUPPRESSING THERMAL TRANSPORT

Beyond electrical performance, thermal transport plays an equally decisive role in determining the thermoelectric figure of merit. The total thermal conductivity (κ_T) comprises two distinct contributions: the electronic thermal conductivity (κ_e) and the lattice thermal conductivity (κ_L). According to the Wiedemann-Franz law, κ_e is intrinsically coupled to electrical conductivity through the Lorenz number[91], meaning that any enhancement in electrical transport inevitably increases κ_e. In contrast, κ_L remains largely independent of electronic transport and therefore offers the most direct and effective pathway for decoupling the competing electrical and thermal parameters. Physically, κ_L reflects phonon transport and is highly sensitive to the composition, crystal structure, lattice defects, and microstructural features of thermoelectric materials[100]. This establishes the optimization of thermal performance through the engineering of structural defects as a primary objective, and numerous strategies have been developed to suppress κ_L, thereby paving the way for significant *ZT* enhancements in advanced thermoelectric systems[101].

Defect engineering

Introducing defects into the GeTe matrix is the primary strategy for diminishing lattice thermal conductivity. Different defect types generally scatter phonons at different frequencies, although the actual frequency range depends on defect size, strain field, density, interface coherence, and phonon dispersion[102]. The spectral lattice thermal conductivity (κ_s) calculated using the Debye-Callaway model for different phonon-scattering mechanisms [Figure 6A] shows that phonons at different frequencies are sensitive to defects of different length scales[103]. For example, point defects scatter high-frequency phonons most effectively, while dislocations, stacking faults, and nanoprecipitates serve as efficient scattering centers for medium-frequency phonons. Grain boundaries and domain boundaries preferentially scatter low-frequency phonons. Thus, constructing multiscale (hierarchical) defects ranging from atomic to microscale in the GeTe matrix can effectively scatter wide-frequency phonons, contributing to extremely low lattice thermal conductivity[104].

Vacancy manipulation converts intrinsic Ge vacancies from point defects, which scatter only high-frequency phonons, into ordered planar defects, vacancy clusters, and dislocations that enable wide-frequency phonon scattering [Figure 6B][105]. Among these transformations, vacancies can accumulate to form nanoscale van der Waals gaps (originating from planar defects): Yu *et al.* formed planar van der Waals gaps by condensing Ge vacancies via Bi and Re doping, and these "quantum gap" defects create nanosized potential wells that enable efficient carrier transmission and selective phonon scattering [Figure 6C], thereby drastically reducing the lattice thermal conductivity and significantly enhancing the thermoelectric performance[106]. Alternatively, vacancies can also accumulate into clusters and dislocation loops. Jiang *et al.* sintered Bi-doped GeTe at 723 and 873 K to control the state of the supersaturated Ge vacancies [Figure 6D][105]. At 723 K, the vacancies remain largely isolated and uniformly distributed, and only a low density of nanoscale defects is observed. At 873 K, the higher vacancy supersaturation drives the aggregation of vacancies into clusters, which collapse into edge dislocation loops; at the same time, positively charged vacancies attract domain walls to form hierarchical nanodomains. These defects scatter phonons over a wide frequency range and thus reduce the lattice thermal conductivity.

Alloying with secondary compounds has proven effective for introducing multiscale defects to scatter phonons in GeTe-based thermoelectrics[83,107]. This relies on the formation of hierarchical defect structures, ranging from atomic-scale point defects and planar vacancies to nanoscale precipitates, dislocations, and

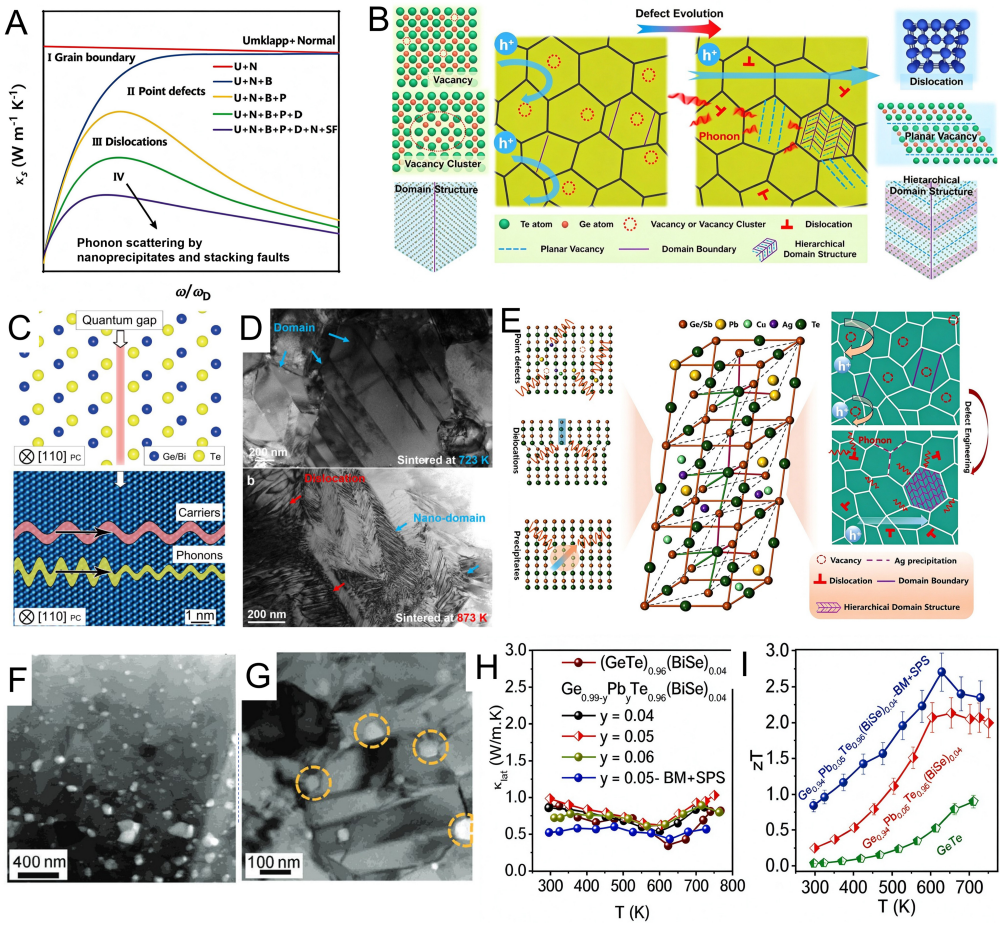

Figure 6. (A) Calculated κ_s by the Debye-Callaway model with different phonon scattering mechanisms; (B) Schematic illustration of the evolution of Ge-vacancy defects and carrier and phonon transport after high-temperature sintering[105]; (C) Structural model of a quantum gap in a Ge-Bi-Te alloy viewed along the $[110]_{PC}$ zone axis; the quantum gap allows carriers to pass through while strongly scattering phonons. Figure 6C is adapted from Ref.[106] under the CC BY 4.0 license; (D) Low-magnification transmission electron microscopy (TEM) images of the Ge-deficient samples sintered at 723K and 873K, respectively. Figure 6B and D is adapted from Ref.[105] under the CC BY 4.0 license; (E) Schematic diagram illustrates the phonon scattering introduced by defect engineering. Figure 6A and E is adapted from Ref.[103] with permission. Copyright © 2024 Wiley; (F) Bright-field scanning transmission electron microscopy (STEM) image of $Ge_{0.94}Pb_{0.05}Te_{0.96}(BiSe)_{0.04}$ sample indicating the grain size distribution; (G) STEM image showing the presence of intragrain 2D defects and the Ge at the grain boundaries; The temperature-dependent (H) lattice thermal conductivity and (I) *ZT* of $Ge1\text{-}xPb_xTe_{0.96}(BiSe)_{0.04}$ samples. Figure 6F-I is adapted from Ref.[110] with permission. Copyright © 2025 Wiley. *ZT*: Dimensionless figure of merit.

phase boundaries, which collectively scatter phonons over a wide frequency range[108]. Li *et al.* introduced $AgSbTe_2$ into $Ge_{0.93}Bi_{0.05}Te$, generating domain structures, dislocations, and phase boundaries that collectively reduced the lattice thermal conductivity to ~ 0.5 W m^{-1} K^{-1}[109]. Jin *et al.* employed CdSe alloying in $Ge_{0.9}Sb_{0.1}Te$, which introduced nanoscale CdSe precipitates, strain fields, and mass fluctuations, leading to strong phonon scattering and substantially suppressed lattice thermal conductivity[99]. Wu *et al.* adopted a combined Sb-Pb and AgCuTe codoping strategy, where AgCuTe alloying introduced dislocations, stacking faults, grain boundaries, and Cu/Ag nanoprecipitates [Figure 6E]. These multiscale defects suppressed the lattice thermal conductivity to 0.42 W m^{-1} K^{-1}[103].

Ball milling can simultaneously introduce inhomogeneous ferroelectric instability, refine grain size, and generate a rich array of nano/mesoscale defects, which is another effective way to construct multiscale defect architectures[110]. Sarkar *et al.* reported that the ball-milling and spark-plasma sintering (BM+SPS) process refined the grain size to 150-400 nm [Figure 6F], introduced amorphous Ge precipitates (50-100 nm) [Figure 6G], intragrain planar defects, and Pb/Se segregation at grain boundaries, all of which synergistically scatter

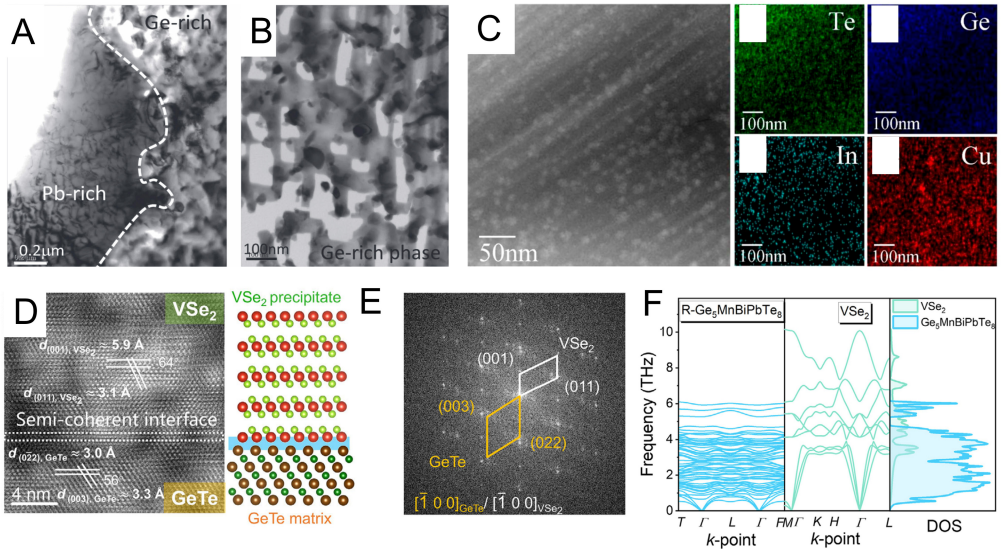

Figure 7. (A) TEM images showing phase separation into Ge-rich and Pb-rich regions, together with a higher-magnification TEM image of the Ge-rich region; (B) Higher magnification of the Ge-rich area. Figure 7A and B is adapted from Ref.[112] with permission. Copyright © 2013 Wiley; (C) High-angle annular dark-field (HAADF)-STEM image indicating the distribution of Cu_2Te nanocrystals and corresponding energy-dispersive X-ray spectroscopy (EDS) elemental mappings. Figure 7C is adapted from Ref.[115] with permission. Copyright © 2021 American Chemical Society; (D) High-resolution transmission electron microscopy (HRTEM) image and the schematic atomic model of the semi-coherent interface; (E) Corresponding fast Fourier transform (FFT) pattern of the $VSe_2/Ge_{0.82}Mn_{0.04}Bi_{0.04}Pb_{0.1}Te$ interface; (F) Phonon spectra of $Ge_5MnBiPbTe_8$ and VSe_2, along with a comparison of their phonon DOS. Figure 7D-F is adapted from Ref.[12] under the CC BY 4.0 license. TEM: Transmission electron microscopy; STEM: scanning transmission electron microscopy; DOS: density of states.

phonons across a broad frequency spectrum, finally leading to a low lattice thermal conductivity of ~ 0.5 W m^{-1} K^{-1} at 300 K and a high *ZT* of ~ 2.7 at 628 K [Figure 6H and I][110]. Sarkar *et al.* demonstrated that the BM+SPS process generates a rich hierarchy of defects spanning multiple length scales: atomic-scale point defects from Sb substitution, 5-20 nm Ge and $GeSb_4Te_7$ nanoprecipitates, 80-200 nm nano/mesoscale grains, and micron-sized Ge precipitates. This all-scale hierarchical architecture effectively scatters phonons across a broad mean free path range, drastically reducing the lattice thermal conductivity to ~ 0.59 W m^{-1} K^{-1} at 723 K[111].

Phase interface engineering

Exploiting the miscibility gap in the PbTe-GeTe phase diagram to achieve controlled phase separation (nucleation and growth) is an effective strategy for introducing hierarchical microstructures. Following this approach, Gelbstein *et al.* successfully incorporated multiscale phase interfaces ranging from 50-100 nm Ge-rich nanoprecipitates to ~ 1 μm PbTe-rich precipitates into GeTe [Figure 7A and B][112]. These multiscale phase interfaces enable wide-frequency phonon scattering and significantly reduce the lattice thermal conductivity from ~ 1.6 to ~ 0.4 W m^{-1} K^{-1}.

By exploiting the low solubility limit of certain elements within the matrix, excessive doping induces secondary phase precipitation and simultaneously perturbs the intrinsic defect equilibrium, thereby introducing dense phase interfaces and defects that range from atomic to micron scales[113,114]. Following this approach, Xie *et al.* introduced Fe into GeTe. Because Fe has negligible solubility in GeTe, it reacts with Ge to form $FeGe_2$ precipitates and generates a high density of Ge planar defects (stacking faults), reducing the lattice thermal conductivity to 0.50 W m^{-1} K^{-1}[113]. Similarly, Zhang *et al.* employed Cu overdoping and In resonant-level doping in GeTe. The excess Cu (up to 12.5-15 at%), which exceeds the solubility limit of ~ 2%, precipitates as Cu_2Te nanocrystals (2-5 nm) and simultaneously fills Ge vacancies [Figure 7C][115]. The strong phonon scattering caused by point defects, Cu_2Te nanocrystals, and associated dislocations leads to an ultralow lattice thermal conductivity of 0.31 W m^{-1} K^{-1}, which is below the amorphous limit of GeTe[115].

Interfacial phonon mismatch arises from phonon DOS differences across heterointerfaces, which block heat-carrying phonons and enhance Kapitza resistance; lower spectral overlap gives stronger blocking[12]. Yin *et al.* introduced VSe_2 nanowires (~ 120 nm wide, several micrometers long) into $Ge_{0.82}Mn_{0.04}Bi_{0.04}Pb_{0.1}Te$[12]. The semi-coherent interfaces with small lattice mismatch (6.25%) and few dislocations [Figure 7D and E] minimize carrier scattering while introducing strong phonon frequency mismatch [Figure 7F].

Introducing a nanoscale second phase with a large thermal expansion mismatch not only creates large phase interfaces but also generates high-density dislocations that scatter phonons. Jiang *et al.* incorporated amorphous boron into Bi-doped GeTe ($Ge_{0.94}Bi_{0.06}Te$) by mechanical alloying and spark plasma sintering[96]. The thermal-expansion-coefficient (TEC) mismatch between boron (~ 1-8 × 10^{-6} K^{-1}) and GeTe (~ 5.6 × 10^{-5} K^{-1}) produces ~ 2.5% misfit strain upon cooling from 873 K, converting vacancies into dense dislocations along the boron/GeTe interfaces that effectively scatter mid-frequency phonons[96].

Nanostructural engineering

Ultrafine ferroelectric domains, obtained by refining the intrinsic 71°/109° domains of rhombohedral GeTe, provide an effective route to suppress the lattice thermal conductivity[75,116,117] [Figure 8A]. In $Ge_{1-x-y}Bi_xCa_yTe$, the large atomic-radius mismatch between Bi and Ca strongly distorts the lattice, refining the ferroelectric domains to an average width of ~ 5 nm, about 20 times smaller than the average domain width in pristine GeTe [Figure 8B], which enhances acoustic phonon scattering and lowers κ_L to 0.48 W m^{-1} K^{-1} at 823 K[75]. First-principles calculations further show that polarization-driven distortions at domain walls reduce κ_L relative to a single crystal[118]. In Bi_2Te_3-alloyed GeTe, Ge vacancies additionally evolve into nanoscale van der Waals gaps that induce 180° nanoscale ferroelectric domain boundaries; both scatter low-frequency phonons below 5 THz, giving a peak ZT of ~2.4 at 773 K[117].

Nanopores and nanovoids offer an additional route to suppress the lattice thermal conductivity. Because phonons cannot propagate across a void, a pore whose size is comparable to the phonon mean free path scatters phonons independently of the surrounding lattice, mainly in the low- and medium-frequency range[100]. Nanopores/nanovoids can form in the hot-pressed $Ge_{0.92}Bi_{0.06}Ga_{0.02}Te$+1.5%Te-BM sample [Figure 8C and D]. The extrusion of excess Te during sintering leaves nanopores mainly at the grain boundaries, leading to a minimum lattice thermal conductivity of 0.43 W m^{-1} K^{-1} at 603 K (about 26% lower than that of the nanopore-free sample) and a peak ZT of 2.6 at 703 K[119]. Similarly, as shown in Figure 8E, nanopores/nanovoids can also be generated by high-energy ball milling or annealing through thermal-expansion mismatch[120,121]. Compared with Ge-vacancy clusters, van der Waals gaps, and nanoprecipitates, nanopores are three-dimensional voids without lattice registry with the matrix. It is worth noting that a certain nanopore/nanovoid content (corresponding to a relative density of 98%-99% in GeTe) does not significantly affect carrier transport, including carrier mobility and concentration[95].

Modular compounds with natural heterostructures reach ultralow lattice thermal conductivity via strong interfacial phonon scattering. These coherent, compositionally modulated nanodomains share the host lattice yet scatter phonons without degrading carrier transport[122]. In Bi-Cd-I triple-doped GeTe ($Ge_{0.93}Bi_{0.04}Cd_{0.03}Te_{0.96}I_{0.04}$), Li *et al.* induced dense Ge vacancies that aggregate into clusters and drive spinodal decomposition during sintering, yielding coherent, heavily doped nanodomains with an ultralow lattice thermal conductivity of 0.33 W m^{-1} K^{-1}[123].

Nanotwin architecture, a dense array of coherent twin boundaries, can scatter phonons while preserving electrical transport[113,124-126]. Li *et al.* constructed dense nanotwins by alloying $(GeTe)_{0.93}(CuBiS_2)_{0.07}$ with 7 mol% $CuBiS_2$, which introduced numerous twin boundaries and substantial lattice strain into the GeTe matrix [Figure 8F][82]. Twin boundaries mainly scatter low- and mid-frequency phonons and point defects

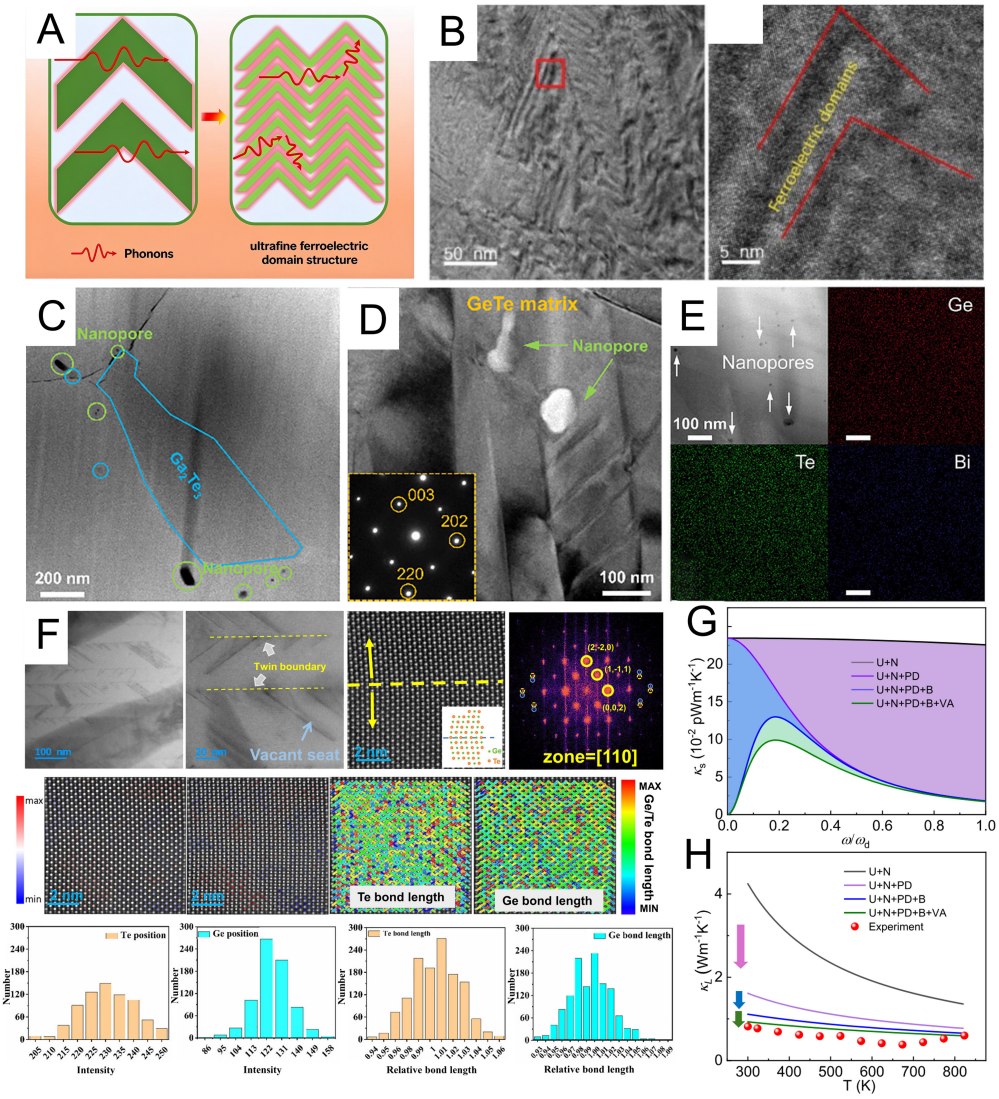

Figure 8. (A) Diagram illustrating phonon scattering by an ultrafine ferroelectric-domain structure; (B) TEM image of ultrafine ferroelectric domains in the $Ge_{0.85}Bi_{0.09}Ca_{0.06}Te$ sample. Figure 8A and B is adapted from Ref.[75] with permission. Copyright © 2023 American Chemical Society; (C) HAADF image revealing the presence of nanopores in the $Ge_{0.92}Bi_{0.06}Ga_{0.02}Te$ + 1.5%Te-BM bulk matrix; (D) Higher magnification of the nanopores. Figure 8C and D is adapted from Ref.[119] with permission. Copyright © 2025 American Chemical Society; (E) TEM image showing the nanopores in the $Ge_{0.94}Bi_{0.06}Te$-BM-t sample. Figure 8E is adapted from Ref.[121] with permission. Copyright © 2026 Wiley; (F) Twin structures and local lattice distortions in $(GeTe)_{0.93}(CuBiS_2)_{0.07}$ revealed by atomic-scale microscopy; (G) Spectral lattice thermal conductivity (κ_s) calculated using the Debye-Callaway model for different phonon-scattering mechanisms at 300 K; (H) Calculated κ_L values from the Debye-Callaway model, including different scattering mechanisms, compared with the experimental values for the $(GeTe)_{0.93}(CuBiS_2)_{0.07}$ sample. Figure 8F-H is adapted from Ref.[82] under the CC BY 4.0 license. TEM: Transmission electron microscopy; HAADF: High-angle annular dark-field; BM: ball milling.

scatter high-frequency phonons [Figure 8G], synergistically yielding an ultralow lattice thermal conductivity of ~ 0.38 W m^{-1} K^{-1} at 673 K [Figure 8H], approaching the theoretical minimum. In addition, combining localized crystal imperfections with phase-diagram engineering in $Bi_{0.1}Ge_{0.9}Te$ can also produce hierarchical twinning accompanied by dense stacking faults[125].

Collectively, these strategies can effectively suppress lattice thermal conductivity through defect engineering, phase-interface engineering, and nanostructural engineering. The central trade-off is that most phonon-scattering centers also scatter carriers, so that a reduction in the lattice thermal conductivity is normally accompanied by a loss of carrier mobility. Coherent defects, such as twin boundaries, low-angle domain

boundaries, and modular nanodomains, scatter phonons while largely preserving carrier transport. To compensate for the degradation of carrier transport caused by microstructural design, it is necessary to combine these approaches with electrical optimization (vacancy engineering, band engineering, and symmetry manipulation) to improve GeTe performance synergistically.

ADVANCES IN THERMOELECTRIC DEVICES AND SERVICE RELIABILITY

GeTe-based thermoelectric devices

Recent breakthroughs in the performance optimization of GeTe thermoelectric materials have created significant opportunities for device fabrication and practical applications. The fabrication of thermoelectric devices represents a critical step toward the commercialization of thermoelectric technology, and enhancing device-level conversion efficiency remains the central research focus in this field. The theoretical maximum conversion efficiency of a material is given by[44]:

$$ZT_{ave} = \frac{1}{T_h - T_c}\int_{T_c}^{T_h} ZT\,dT \tag{2}$$

$$\eta_{\max} = \frac{T_h - T_c}{T_h}\frac{\sqrt{1+ZT_{ave}} - 1}{\sqrt{1+ZT_{ave}} + T_c/T_h} \tag{3}$$

In actual thermoelectric energy conversion, the conversion efficiency is substantially lower than the theoretical value due to material instability, heat-flow losses, internal resistance arising from interface barrier layers, and elemental interdiffusion at solder joints[127]. Therefore, the actual conversion efficiency is measured using a thermoelectric-device testing platform, where the output voltage U, the output current I, and the heat flow at the cold side Qc are recorded; the output power P and the conversion efficiency η are calculated using[128]:

$$P = U \times I \tag{4}$$

$$\eta = \frac{P}{P + Q_c} \times 100\% \tag{5}$$

Single-leg devices serve as fundamental platforms to evaluate intrinsic material potential and interfacial contact quality. Notable conversion efficiencies have been achieved in single-leg GeTe-based thermoelectric devices. For example, the $(CoGe_2)_{0.01}Ge_{0.85}Sb_{0.10}Te$ sample reached an max of 8.2% at ΔT = 420 K[129], the $Ge_{0.78}In_{0.005}Ga_{0.005}Pb_{0.1}Sb_{0.07}Te$ sample achieved an max of 13.5% at ΔT = 450 K[94], the $(Ge_{0.98}Cu_{0.04}Te)_{0.88}(PbSe)_{0.12}$ sample realized an max of 14% at ΔT = 440 K[130]. A record-high single-leg device efficiency of 15.7% was achieved at ΔT = 460 K for the $(Ge_{0.82}Mn_{0.04}Bi_{0.04}P_{b0.1}Te)_{0.99}(VSe_2)_{0.01}$ sample, representing an important milestone for practical materials evaluation[12].

The device efficiency is strongly correlated with the average ZT (ZT_{avg}). Segmented thermoelectric devices, composed of different thermoelectric materials from the hot to cold side, can take full advantage of the high ZT of each thermoelectric material over its optimized temperature range, thereby providing an effective way to boost the ZT_{avg} and η_{max}[131]. The state-of-the-art Bi_2Te_3-based alloys are typically used on the cold side. Pei *et al.* fabricated a GeTe/$(Bi, Sb)_2Te_3$ segmented one-leg thermoelectric (TE) module with Ti-Ni diffusion barriers, which showed an max of 9.5% at ΔT = 423 K[131]. Further, Geng *et al.* realized one-step-sintered GeTe/Bi_2Te_3 segmented legs using Al-Si-Ni diffusion barriers, attaining 15.5% efficiency at ΔT = 449 K while addressing critical interface-mismatch and thermal-stability challenges[132]. Single-leg device efficiency does not directly reflect the performance of actual thermoelectric modules, which are additionally constrained by thermal-expansion mismatch and p-n matching.

Multi-pair thermoelectric devices, assembled by electrically connecting multiple p-n couples in series and thermally in parallel between ceramic substrates, serve as the core practical platform for heat-to-electricity conversion beyond single-leg prototypes[83]. Recent studies have reported notable progress in multi-pair GeTe-based thermoelectric devices. CuAgSe-alloyed $Ge_{0.92}Sb_{0.08}Te$ delivered 6.0% efficiency at ΔT = 382 K in a seven-pair module,[83] MXene-composited $Ge_{0.93}Bi_{0.07}Te$ reached 7.5% at ΔT = 300 K in a seven-pair setup,[98] phase-stabilized cubic $Ge_{0.7}Mn_{0.21}Sb_{0.09}Te$ with Co barriers attained 12.2% at ΔT = 480 K in a two-pair segmented device[133], negative-enthalpy-stabilized $Ge_{0.79}Mg_{0.06}Cu_{0.04}Sb_{0.04}Pb_{0.09}Te$ achieved a record 16.0% at ΔT = 520 K in an eight-pair TE device[134].

Together, these three device categories represent a progression from material evaluation to practical power generation: a single-leg device reflects the intrinsic ZT_{avg} and the interfacial quality of the material, a segmented device extends the high-ZT temperature window to raise ZT_{avg}, and a multi-pair module converts performance improvements into practical output. In every category, the most effective strategies are those that raise ZT and ZT_{avg}. Nevertheless, the measured conversion efficiency is always lower than the theoretical or simulated values, mainly because of (i) interfacial contact resistances aggravated by interfacial reaction layers and solder-joint interdiffusion, (ii) heat-flow losses that increase with ΔT, (iii) microcracking induced by thermal-expansion mismatch and the phase transition under thermal cycling, and (iv) non-ideal leg geometry and p-n matching. We have summarized the efficiencies of representative GeTe-based thermoelectric devices in Table 1. The table also lists the ZT values of the p-type legs and the corresponding electrode configurations. The table shows that materials with the same peak ZT can exhibit noticeably different efficiencies depending on the temperature difference and electrode material[25]. Thus, narrowing this efficiency gap is the central task for practical GeTe devices, with optimized interfacial contact materials, matched thermal expansion, and optimized leg geometry playing a decisive role.

Service reliability

In addition to high material performance and successful device fabrication, practical applications require robust mechanical properties, high thermal-cycling stability, and reliable devices[142].

Hardness and strength are key mechanical properties for assessing the machinability and service reliability of thermoelectric materials. Pristine GeTe exhibits relatively modest hardness (~ 116 H_v) and compressive strength (~ 150 MPa)[143]. To overcome these limitations, Sb doping of GeTe can suppress Ge vacancies and microcrack propagation, and combined with SPS-induced grain refinement, the hardness can be enhanced to ~ 186 H_v[143]. Moreover, introducing multiscale defects into the GeTe matrix not only significantly reduces lattice thermal conductivity but also effectively impedes crack propagation, leading to a substantial improvement in Vickers hardness[136,144-146]. For instance, solid-solution strengthening, precipitation strengthening, and grain-boundary strengthening induced by MgB_2 alloying result in a compressive strength of ~ 271 MPa and a Vickers hardness of ~ 236 H_v[147]. The synthesis of high-entropy GeTe thermoelectric materials also yields a marked increase in hardness. For example, medium-entropy GeTe achieved through co-doping of Mn, Pb, Sb, and Cd exhibits a significantly enhanced hardness of ~ 270 H_v[148]. Furthermore, nanoscale twin boundaries in GeTe effectively block dislocation motion [Figure 9A]. Dislocations can also be pinned at nanoscale twin boundaries and react with other dislocations to form stable, immobile dislocation locks. This significantly increases the hardness to 224 H_v and the compressive strength to 350 MPa [Figure 9B and C][82,148] However, a high nanopore content in GeTe can deteriorate its hardness and compressive strength. This occurs because the formation of nanopores/nanovoids leads to a loss of contact between grains in the matrix and weakens interfacial adhesion[100]. In addition, nanopores/nanovoids act as stress concentrators, leading to the formation and propagation of cracks. In terms of thermal-cycling stability, pores are expected to act as preferential sites for crack initiation and propagation, thereby degrading the long-term reliability of GeTe-based devices[100,120].

Table 1. Reported efficiencies of representative GeTe-based thermoelectric devices

Composition	Device type	η_{max} (%)	ΔT (K)	*ZT* of the p-type leg	Electrode
$(CoGe_2)_{0.01}Ge_{0.85}Sb_{0.10}Te$[129]	single-leg	8.2	420	ZT_{max} ~ 2.2 @775 K; ZT_{avg} 1.2 (300-775 K)	/
$Ge_{0.78}In_{0.005}Ga_{0.005}Pb_{0.1}Sb_{0.07}Te$[94]	single-leg	13.5	450	ZT_{max} ~ 2.1 @773 K; ZT_{avg} ~ 1.43 (300-773 K)	/
$(Ge_{0.98}Cu_{0.04}Te)_{0.88}(PbSe)_{0.12}$[130]	single-leg	14.0	440	ZT_{max} ~ 2.5; ZT_{avg} 1.8 (300-800 K)	Ag
$(Ge_{0.82}Mn_{0.04}Bi_{0.04}Pb_{0.1}Te)_{0.99}(VSe_2)_{0.01}$[12]	single-leg	15.7	460	ZT_{max} 2.7 @773 K; ZT_{avg} ~ 1.9 (300-773 K)	Ag
$Ge_{0.87}Y_{0.02}Sb_{0.10}Ag_{0.01}Te$[66]	single-leg	13.4	463	ZT_{max} ~ 2.7; ZT_{avg} ~ 1.73 (323-773 K)	Fe
$(GeTe)_{0.93}(CuBiS_2)_{0.07}$[82]	single-leg	12.0	470	ZT_{max} ~ 2.5; ZT_{avg} 1.9 (400-823 K)	Cu
$(GeTe)_{0.90}(CuBiSe_2)_{0.03}(PbTe)_{0.07}$[135]	single-leg	13.4	473	ZT_{max} ~ 2.0; ZT_{avg} 1.4-1.5 (400-773 K)	Ni (hot) / Cu (cold)
$Ge_{0.78}Cd_{0.06}Pb_{0.1}Sb_{0.06}Te$[136]	single-leg	5.2	250	ZT_{max} 1.76 @553 K; ZT_{avg} 1.18 (303-553 K)	/
$GeTe/(Bi,Sb)_2Te_3$[131]	segmented	9.5	423	ZT_{max} 1.9 (623-723 K)	Cu
$GeTe/Bi_2Te_3$[132]	segmented	15.5	449	/	Cu
boron-dispersed $GeTe/(Bi,Sb)_2Te_3$[96]	segmented	13.7	455.9	ZT_{max} 2.45; ZT_{avg} 1.1 (300-613 K)	/
$Ge_{0.61}Ag_{0.11}Sb_{0.13}Pb_{0.12}Bi_{0.01}Te/Bi_2Te_3$-based[11]	segmented	13.3	506	ZT_{max} ~ 2.7	/
$Bi_{0.5}Sb_{1.5}Te_3/GeTe$[137]	segmented	13.6	493	/	/
cubic-$GeTe/Mg_3(Sb,Bi)_2$[138]	segmented (2-pair module)	12.8	480	ZT_{avg} ~ 1.16-1.23	/
$Ge_{0.7}Mn_{0.21}Sb_{0.09}Te$[133]	segmented (2-pair module)	12.2	480	ZT_{max} 1.73 @773 K; ZT_{avg} 1.0	Cu
$Ge_{0.79}Mg_{0.06}Cu_{0.04}Sb_{0.04}Pb_{0.09}Te$[134]	segmented (8-pair module)	16.0	520	ZT_{max} 2.7 @800 K; ZT_{avg} ~ 1.6 (300-800 K)	Ag
CuAgSe-alloyed $Ge_{0.92}Sb_{0.08}Te$[83]	multi-pair (7-pair module)	6.0	382	ZT_{max} 2.02 @603 K; ZT_{avg} 1.22 (303-803 K)	/
MXene-composited $Ge_{0.93}Bi_{0.07}Te$[98]	multi-pair (7-pair module)	7.5	300	ZT_{max} ~ 2.1 @603 K; ZT_{avg} ~ 1.1	/
$Ge_{0.89}Cu_{0.06}Sb_{0.08}Te/Yb_{0.3}Co_4Sb_{12}$[139]	multi-pair (8-pair module)	12.0	545	ZT_{max} 1.7	Mo-Cu (hot) / Cu (cold)
$(Ge_{0.96}Bi_{0.04}Te)_{0.96}(CuI)_{0.04}/Bi_2Te_{2.7}Se_{0.3}$[140]	multi-pair (17-pair module)	8.6	400	ZT_{max} 2.0 @700 K; ZT_{avg} 1.3 (300-700 K)	Cu
$Ge_{0.78}Ga_{0.01}Pb_{0.1}Sb_{0.07}Te/Yb_{0.3}Co_4Sb_{12}$[93]	multi-pair (18-pair module)	5.9	476	ZT_{max} ~ 2.1 @773 K; ZT_{avg} ~ 1.3 (300-773 K)	Cu
$Ge_{0.92}Sb_{0.04}Bi_{0.04}Te_{0.95}Se_{0.05}/Yb_{0.3}Co_4Sb_{12}$[40]	multi-pair (8-pair module)	7.8	500	ZT_{max} 2.0 @700 K	Ni
$(Ge_{0.89}Pb_{0.08}Bi_{0.03}Te)_{0.97}(HgTe)_{0.03}$[78]	multi-pair (7-pair module)	10.8	500	ZT_{max} 2.31 @650 K; ZT_{avg} 1.52 (300-773 K)	/
$(GeTe)_{78}(Ag_{0.77}Sb_{1.23}Te_{2.23})_{22}/Pb_{0.985}Sb_{0.015}Te$[141]	multi-pair (8-pair module)	6.3	480	ZT_{max} ~ 2.0 @673 K	/

η_{max} denotes the maximum efficiency, and ΔT denotes the temperature difference between the cold and hot sides. "/" indicates that the electrode is not specified in the cited work. *ZT*: Dimensionless figure of merit.

Thermal cycling stability ultimately determines the service life of GeTe-based devices, and it is governed mainly by the smoothness of the volume change across the phase transition. When the volume change is abrupt, cycling causes severe degradation. The rhombohedral-to-cubic phase transition at approximately 670 K degrades the reliability of the material and the device[24]. Suppressing the phase transition is essential for enhancing the thermal-cycling stability of GeTe-based materials[149]. Since the transition is driven by the Peierls distortion, weakening this distortion to lower the phase-transition temperature is necessary.

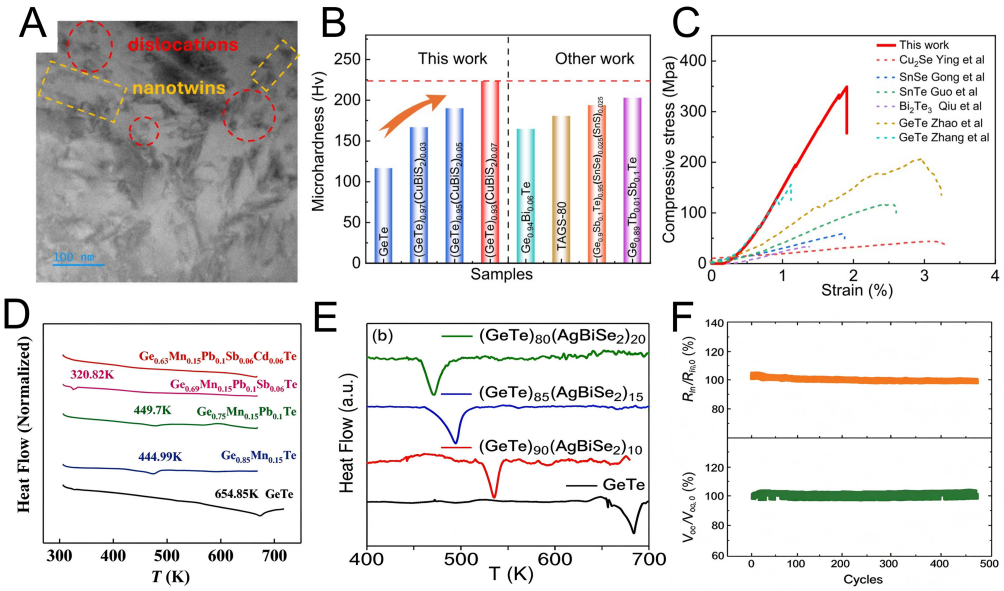

Figure 9. (A) Annular bright-field (ABF)-STEM strain contrast image showing nanotwins (yellow frames) and associated dislocations (red circles) among them; (B) The Vickers microhardness (H_v) of $(GeTe)_{1-x}(CuBiS_2)_x$ samples, compared with literature data; (C) Compressive stress-strain curves compared with those of representative TE materials. Figure 9A-C is adapted from Ref.[82] under the CC BY 4.0 license; (D) DSC curves show that the phase-transition temperature decreases with increasing configurational entropy. Figure 9D is adapted from Ref.[148] under the CC BY 4.0 license; (E) DSC signal as a function of temperature, showing the decrease in phase-transition temperature with increasing $AgBiSe_2$ alloying concentration. Figure 9E is adapted from Ref.[151] with permission. Copyright © 2019 American Chemical Society; (F) Internal resistance and open-circuit voltage of the Ni/Ti diffusion barrier measured during the thermal-cycling test. Figure 9F is adapted from Ref.[9] under the CC BY 4.0 license. STEM: Scanning transmission electron microscopy; DSC: differential scanning calorimetry; TE: thermoelectric.

High-entropy design, as illustrated in Figure 9D, can achieve this by increasing configurational entropy, reducing Ge atomic displacement, and weakening the Peierls distortion[11,148,150]. Such suppression can also be achieved by alloying. As shown in Figure 9E, increasing the $AgBiSe_2$ content continuously decreases the phase-transition temperature of GeTe[151]. Similar suppression of the phase transition has been reported in GeTe alloyed with $AgSbTe_2$[141], MnTe[88], $LiBiTe_2$[152], and MgB_2[147]. For instance, MgB_2 alloying induces partial substitution of Mg for Ge[147], which suppresses the phase transition; meanwhile, B segregates at grain boundaries, refining the grains. This results in a smooth dL/L_0 curve across the phase-transition temperature and alleviates thermal-cycling stress in devices. The $Ge_{0.7}Mn_{0.21}Sb_{0.09}Te$ sample achieved a phase-stabilized cubic structure and completed 50 thermal cycles between 473 and 773 K, with all key performance indicators remaining stable and showing negligible degradation[133]. These results indicate that suppressing the volume change at the transition enhances thermal-cycling stability.

Device stability ultimately determines the service life of a GeTe-based module, and it is governed mainly by the quality of the electrode/leg interface. If the diffusion barrier is not optimized, reaction layers and elemental interdiffusion increase the interfacial resistance during operation, causing the conversion efficiency to decay accordingly[25]. A suitable barrier must therefore combine low contact resistivity, a thermal expansion coefficient close to that of the leg, and a slow interfacial reaction. Since high-efficiency devices require a contact resistance below approximately 1 cm^2, interface engineering remains a principal source of the gap between material-level ZT and device-level efficiency[132]. For GeTe, various metals have been screened as candidate barriers. The Ni barrier maintains low interfacial resistivity, but its thermal-expansion mismatch with GeTe causes the legs to crack during manufacturing. Thermal expansion of the barrier is equally important. Ti, whose linear expansion coefficient (10.8×10^{-6} K^{-1}) is close to that of GeTe, provides a contact resistance of 3 cm^2 together with a diffusion layer only 0.4 μm thick, whereas $Al_{66}Si_{34}$ reacts strongly

with Te and gives 20.6 cm^2[131,132]. A Ni/Ti diffusion barrier for GeTe, which combines the advantages of Ni and Ti, retained a stable internal resistance and open-circuit voltage after 450 thermal cycles between 473 and 800 K [Figure 9F][9]. Overall, developing suitable barriers that provide low interfacial contact resistance and minimize thermal-expansion mismatch is essential for device-level stability.

N-TYPE GETE THERMOELECTRICS

Most research on GeTe thermoelectric materials focuses on p-type GeTe because n-type GeTe exhibits poor thermoelectric performance for several fundamental reasons. First, the high hole carrier concentration of ~ 10^{21} cm^{-3} for intrinsic GeTe originates from abundant Ge vacancies and makes it difficult to achieve n-type electron transport[153]. Second, unlike the multiple converging valence-band edges, the conduction-band minimum lies at the L point and is dominated by Ge 4p states[14,101]. Thus, n-type conduction requires chemical modification of the conduction band (e.g., Bi-p states). Third, the narrow band gap (~ 0.25 eV) causes a strong bipolar effect and restricts the operating temperature of n-type GeTe to below ~ 525 K, in contrast to 500-800 K for p-type GeTe[154]. Developing high-performance n-type GeTe is crucial for constructing all-GeTe thermoelectric modules with well-matched p- and n-type legs, yet it remains one of the most challenging tasks in the field.

Realizing n-type GeTe requires reversing the majority-carrier polarity from holes to electrons by compensating the excess holes, followed by the same band and defect engineering used for p-type materials. Representative n-type GeTe examples include $AgBiTe_2$-alloyed $(GeTe)_{0.45}(AgBiTe_2)_{0.55}$ and bipolar suppressed $Ge_{0.46}Bi_{0.17}Pb_{0.37}Te_{0.7}Se_{0.3}$, which achieve a peak ZT of ≈ 0.5 and single-leg efficiencies of 5%-6.6%[153,154]. Nevertheless, the overall performance of n-type GeTe remains far below that of p-type GeTe. Consequently, practical GeTe modules still pair p-type GeTe with mature n-type legs such as $Yb_{0.3}Co_4Sb_{12}$, $Bi_2Te_{2.7}Se_{0.3}$, and PbTe [Table 1], rather than with n-type GeTe. Achieving high performance in n-type GeTe would enable all-GeTe modules with matched thermal expansion, simplified interfaces, and lower cost, representing a crucial step toward practical thermoelectric applications.

GETE THERMOELECTRIC FILMS

GeTe-based thin films are essential for micro-thermoelectric coolers, generators and self-powered sensors, but their thermoelectric performance is generally inferior to that of bulk GeTe and is limited by several film-specific problems. First, GeTe films inherit the high intrinsic hole concentration (~ 10^{21} cm^{-3}) generated by Ge vacancies, which significantly lowers the Seebeck coefficient[155]. Second, grain boundaries, interfaces and structural defects in polycrystalline films scatter carriers and reduce the mobility[156]. In addition, chemical doping used to lower the hole concentration can introduce additional ionized-impurity and alloy-disorder scattering. Balancing the carrier concentration and mobility is therefore more difficult than in bulk GeTe. Third, as-deposited films are often amorphous or poorly crystallized with mixed phases, and the rhombohedral-to-cubic phase transition can further degrade the transport properties[157,158]. Fourth, the strong coupling among the Seebeck coefficient, electrical conductivity and thermal conductivity, together with the anisotropy between in-plane and out-of-plane transport, makes it difficult to simultaneously achieve a high power factor and low thermal conductivity. As a result, the power factor of GeTe films has historically remained below ~ 21 μW cm^{-1} K^{-2}[155].

To overcome these problems, film-specific strategies have been developed. Through control of stoichiometry and self-doping, the hole concentration can be optimized. Ge self-doping through prolonged annealing optimizes the hole concentration to ~ 2.3 × 10^{20} cm^{-3} and raises the Hall mobility to ~ 51 cm^2 V^{-1} s^{-1}[156]. Also, Te-poor epitaxial GeTe films on Si (111) suppress Ge-vacancy generation and reduce the hole concentration to ~ 3 × 10^{20} cm^{-3}[157]. Low-angle and twin boundaries formed by domain engineering can decouple phonon

and carrier transport, while larger grains, higher structural symmetry, and preferred (00l) orientation can reduce grain-boundary carrier scattering, enhance band degeneracy, and increase the DOS effective mass. Controlling the phase and crystallinity is another effective strategy. Annealing improves the crystallinity and reduces grain-boundary scattering, while Sb/In co-doping stabilizes the cubic phase over the working temperature range and Sn doping lowers the temperature required to form the cubic structure[159], both of which are beneficial for achieving a high power factor and low thermal conductivity. Overall, these strategies have raised the power factor of GeTe films to values comparable to or even higher than those of bulk GeTe and have enabled prototype film-based generators[155]. Nevertheless, several challenges remain: the trade-off between phonon and carrier scattering at grain boundaries/interfaces, the reliable measurement of anisotropic thermal transport and *ZT* in films, the stabilization of the cubic phase and interfaces during long-term operation, and the scale-up of film growth and device integration. Addressing these issues, together with the bulk strategies discussed above, will be important for translating the promising film-level results into practical micro-thermoelectric applications.

CONCLUSION AND OUTLOOK

In summary, GeTe has established itself as a premier lead-free thermoelectric material for mid-temperature power generation, with peak *ZT* values exceeding 2.5 achieved through a diverse array of strategies. This review has systematically analyzed the fundamental crystal structure, electronic band structure, and phase-transition behavior, providing a foundation for understanding property optimization. For electrical transport, three synergistic routes have been identified: Optimizing the carrier concentration by aliovalent doping, vacancy-formation-energy enhancement, and non-equilibrium processing effectively reduces the intrinsically high hole density to the optimal range of $1 \sim 3 \times 10^{20}$ cm^{-3}. Carrier mobility enhancement via band sharpening, lattice plainification, and interfacial engineering enables higher electrical conductivity without compromising the Seebeck coefficient. DOS effective mass enhancement through valley degeneracy engineering, crystal symmetry manipulation, resonant-level doping, and energy filtering substantially boosts the Seebeck coefficient and power factor. For thermal transport, multiscale defect engineering has proven exceptionally effective. Strategies such as phase separation, excess doping, alloying with secondary compounds, ball milling, modular nanostructures, nanotwin architectures, interfacial phonon mismatch, lattice anharmonicity enhancement, thermal-expansion-mismatch dislocations, and vacancy manipulation collectively scatter phonons across the entire mean-free-path spectrum, achieving lattice thermal conductivities approaching the amorphous limit (as low as 0.31 W m^{-1} K^{-1}).

Beyond thermoelectric performance, significant progress has been made in mechanical properties and device integration. Hardness and compressive strength have been enhanced to ~ 270 H_v and ~ 350 MPa, respectively, through solid-solution strengthening, grain refinement, and nanotwinning. Stabilizing the cubic phase at room temperature via alloying or high-entropy design eliminates the detrimental phase transition and improves thermal-cycling stability. Importantly, device-level conversion efficiencies have reached record values, up to 16.0% in multi-pair modules, demonstrating the practical potential of GeTe-based thermoelectrics. Recent progress in n-type GeTe and GeTe-based thin films is also summarized, although their performance is still inferior to that of p-type bulk GeTe.

Every optimization strategy has its own strengths and limitations, and the accompanying negative effects must also be weighed. Systematic trade-offs exist among the different optimization strategies. Doping lowers the carrier concentration at the cost of additional point-defect scattering; resonant levels raise the DOS effective mass while depressing the mobility; band convergence and band flattening increase the effective mass at the expense of mobility; phase-transition suppression and mechanical strengthening constrain the lattice and therefore the carrier transport; and every phonon-scattering center also scatters carriers to some extent. A comparative assessment of the main optimization strategies and their limitations is summarized in

Table 2. Comparative assessment of the main optimization strategies and their limitations in GeTe thermoelectrics

Strategy	Key benefit	Main limitation
Carrier concentration optimization (heterovalent doping, vacancy engineering)	Optimizes the hole concentration and power factor	Introduces ionized-impurity scattering
Carrier mobility enhancement (band sharpening, lattice plainification)	Higher conductivity without sacrificing the Seebeck coefficient	Limited by intrinsic vacancy scattering
Band engineering (band convergence, symmetry, resonant levels, energy filtering)	Substantially enhances the Seebeck coefficient and power factor	May lower mobility or narrow the band gap
Thermal transport suppression (multiscale defect engineering)	Reduces lattice thermal conductivity	May impair carrier transport
Phase-transition and mechanical properties (cubic stabilization, dislocation blocking)	Reduces thermal-expansion mismatch and the risk of cracking while improving mechanical strength and thermal-cycling stability	May impair carrier transport

The table summarizes general qualitative trends only; the actual effectiveness of each strategy is strongly dependent on the doping/alloying concentration, the preparation and heat-treatment conditions, and the resulting microstructure, and should not be regarded as an absolute rule or as a quantitative prediction.

Table 2. In practice, a single strategy is not sufficient for achieving high *ZT* values and device efficiencies. Only when complementary strategies of carrier regulation, band engineering, defect engineering, and phase-transition/interface optimization are integrated can we synergistically realize electron-phonon co-optimization.

Outlook and future directions. Despite these impressive advances, several challenges remain: First, the strong coupling between electronic and thermal transport calls for more sophisticated co-optimization strategies that simultaneously enhance power factor and suppress lattice thermal conductivity without compromising mobility. In this regard, data-driven approaches are emerging in GeTe thermoelectric research. High-throughput and first-principles selection of dopants combined with automated computational workflows can accelerate the discovery of optimal dopant combinations[160,161]. Machine learning (ML) and artificial intelligence (AI) have emerged as data-driven complements to experiments and DFT calculations: they learn composition-structure-property relationships from existing experimental and computational datasets and use them to predict properties or screen candidate compositions with fewer trial-and-error iterations[162,163]. Second, the phase-transition issue, though mitigated by alloying, still requires a deeper understanding of the long-term stability and fatigue behavior under thermal cycling, especially for real-world applications. Third, the development of n-type GeTe is still at an early stage, and its thermoelectric performance remains low[153]. Developing n-type GeTe materials with thermoelectric performance comparable to that of p-type GeTe is promising for constructing all-GeTe modules and represents a decisive step toward balanced device design[154]. Fourth, device-level challenges such as interfacial reactions, contact resistance, and elemental diffusion at solder joints need systematic solutions, and scalable, cost-effective processing routes should be further developed to translate high *ZT* into high module efficiency.

DECLARATIONS

Acknowledgments

The graphical abstract includes the following elements: (i) the carrier-mobility illustration was adapted from Ref.[68] under the CC BY 4.0 license, and the DOS effective-mass illustration was adapted from Ref.[76] with permission (Copyright © 2019 American Chemical Society); (ii) the phase-interface engineering illustration was adapted from Ref.[112] with permission (Copyright © 2013 Wiley) and from Ref.[12] under the CC BY 4.0 license; the nanostructural-engineering illustration was adapted from Ref.[82] under the CC BY 4.0 license and from Ref.[75] with permission (Copyright © 2023 American Chemical Society); the defect-engineering illustration was adapted from Ref.[103] with permission (Copyright © 2024 Wiley); (iii) the single-leg and multi-pair device schematics were prepared by the authors; and (iv) the strength/hardness illustration was adapted from Ref.[82], the thermal-cycling stability illustrations were adapted from Refs.[148] and [82], and the device-stability illustration was adapted from Ref.[68], all under the CC BY 4.0 license where indicated.

Authors' contributions

Conception: Li, S.
Design of the study: Li, S.
Data analysis: Li, S.; Geng, Y.; Zhang, Q.
Interpretation: Li, S.; Geng, Y.; Zhang, Q.
manuscript drafting: Li, S.
Figures preparation: Li, S.
Data acquisition: Xu, H.; Tang, G.
Manuscript revision: Tang, G.
Administrative, technical, and material support: Tang, G.

Availability of data and materials

Not applicable.

AI and AI-assisted tools statement

During the preparation of this manuscript, the AI tool DeepSeek (version V4.1-flash, released 2026-06-10) was used solely for language editing. The tool did not influence the study design, data collection, analysis, interpretation, or the scientific content of the work. All authors take full responsibility for the accuracy, integrity, and final content of the manuscript.

Financial support and sponsorship

The work was supported by the National Natural Science Foundation of China (No. 52071182), the "Qinglan Project" of the Young and Middle-aged Academic Leader of Jiangsu Province, and the Fundamental Research Funds for the Central Universities (No. 202510).

Conflicts of interest

Tang, G. is an Associate Editor of *Energy Z* but was not involved in the editorial process, including reviewer selection, manuscript handling, or decision-making. The other authors declare that they have no conflicts of interest.

Ethical approval and consent to participate

Not applicable.

Consent for publication

Not applicable.

Copyright

© The Author(s) 2026.

REFERENCES

1. Gong, Y.; Dou, W.; Lu, B.; et al. Divacancy and resonance level enables high thermoelectric performance in n-type SnSe polycrystals. *Nat. Commun.* **2024**, *15*, 4231. DOI PubMed PMC
2. Li, S.; Iqbal, M. F.; Zhao, C.; et al. Band flattening and localized lattice engineering realized high thermoelectric performance in GeTe. *J. Mater. Chem. A.* **2025**, *13*, 32159-68. DOI
3. Zhang, Q.; Ying, P.; Farrukh, A.; et al. High wide-temperature-range thermoelectric performance in GeTe through hetero-nanostructuring. *Acta. Materialia.* **2024**, *276*, 120132. DOI
4. He, J.; Tritt, T. M. Advances in thermoelectric materials research: looking back and moving forward. *Science* **2017**, *357*, eaak9997. DOI PubMed
5. Dong, J.; Sun, F.; Tang, H.; et al. Medium-temperature thermoelectric GeTe: vacancy suppression and band structure engineering leading to high performance. *Energy. Environ. Sci.* **2019**, *12*, 1396-403. DOI
6. Liu, S.; Wang, W.; Xie, L.; et al. Realizing high thermoelectric performance in GeTe-based alloys without lead addition. *Adv. Funct. Mater.* **2026**, *36*, e10362. DOI

7. Hong, M.; Zou, J.; Chen, Z. G. Thermoelectric GeTe with diverse degrees of freedom having secured superhigh performance. *Adv. Mater.* **2019**, *31*, e1807071. DOI PubMed
8. Zhang, X.; Li, J.; Wang, X.; et al. Vacancy manipulation for thermoelectric enhancements in GeTe alloys. *J. Am. Chem. Soc.* **2018**, *140*, 15883-8. DOI
9. Xing, T.; Song, Q.; Qiu, P.; et al. Superior performance and high service stability for GeTe-based thermoelectric compounds. *Natl. Sci. Rev.* **2019**, *6*, 944-54. DOI PubMed PMC
10. Yu, J.; Liu, X.; Jiang, Y.; et al. Giant ZT enhancement in rhombohedral GeTe-based thermoelectric materials. *Nat. Commun.* **2026**, 17. DOI PubMed PMC
11. Jiang, B.; Wang, W.; Liu, S.; et al. High figure-of-merit and power generation in high-entropy GeTe-based thermoelectrics. *Science* **2022**, *377*, 208-13. DOI
12. Yin, L. C.; Lu, X.; Liu, W. D.; et al. Selective interfacial barriers drive high-performance GeTe thermoelectrics. *Adv. Sci. (Weinh).* **2026**, *13*, e75403. DOI PubMed PMC
13. Yang, L.; Chen, Z.; Dargusch, M. S.; Zou, J. High performance thermoelectric materials: progress and their applications. *Adv. Energy. Mater.* **2018**, *8*, 1701797. DOI
14. Zhang, X.; Bu, Z.; Lin, S.; Chen, Z.; Li, W.; Pei, Y. GeTe Thermoelectrics. *Joule* **2020**, *4*, 986-1003. DOI
15. Hong, M.; Chen, Z. G. Chemistry in advancing thermoelectric GeTe materials. *Acc. Chem. Res.* **2022**, *55*, 3178-90. DOI
16. Jiang, Y.; Yu, J.; Li, H.; Zhuang, H. L.; Li, J. F. Chemical modulation and defect engineering in high-performance GeTe-based thermoelectrics. *Chem. Sci.* **2025**, *16*, 1617-51. DOI PubMed PMC
17. Liu, W.; Wang, D.; Liu, Q.; Zhou, W.; Shao, Z.; Chen, Z. High-performance GeTe-based thermoelectrics: from materials to devices. *Adv. Energy. Mater.* **2020**, *10*, 2000367. DOI
18. Bai, X.; Liu, C.; Li, F.; et al. Tailoring 5s2 lone pair-antibonding orbital interaction by Zr-doping to realize ultrahigh power factor in thermoelectric GeTe. *Chem. Eng. J.* **2023**, *461*, 142069. DOI
19. Wang, L.; Fang, S.; Li, J.; et al. Anomalous enhancement of thermoelectric performance in GeTe with specific interaxial angle and atomic displacement synergy. *Cell. Rep. Phys. Sci.* **2022**, *3*, 101009. DOI
20. Shportko, K.; Kremers, S.; Woda, M.; Lencer, D.; Robertson, J.; Wuttig, M. Resonant bonding in crystalline phase-change materials. *Nat. Mater.* **2008**, *7*, 653-8. DOI PubMed
21. Tsai, Y.; Chao, Y.; Hsing, C.; et al. From stoichiometric to off-stoichiometric GeTe: phase diagram reconstruction and thermoelectric performance reassessment. *Acta. Materialia.* **2024**, *265*, 119644. DOI
22. Rabe, K. M.; Joannopoulos, J. D. Theory of the structural phase transition of GeTe. *Phys. Rev. B. Condens. Matter.* **1987**, *36*, 6631-9. DOI PubMed
23. Gainza, J.; Serrano-Sánchez, F.; Nemes, N. M.; Martínez, J. L.; Fernández-Díaz, M. T.; Alonso, J. A. Features of the high-temperature structural evolution of GeTe thermoelectric probed by neutron and synchrotron powder diffraction. *Metals* **2020**, *10*, 48. DOI
24. Chatterji, T.; Kumar, C. M. N.; Wdowik, U. D. Anomalous temperature-induced volume contraction in GeTe. *Phys. Rev. B.* **2015**, *91*, 054110. DOI
25. Le, W.; Yang, W.; Sheng, W.; Shuai, J. Research progress of interfacial design between thermoelectric materials and electrode materials. *ACS. Appl. Mater. Interfaces.* **2023**, *15*, 12611-21. DOI PubMed
26. Liu, H.; Zhang, X.; Li, J.; et al. Band and phonon engineering for thermoelectric enhancements of rhombohedral GeTe. *ACS. Appl. Mater. Interfaces.* **2019**, *11*, 30756-62. DOI
27. Guo, D.; Li, C.; Qiu, K.; et al. The n- and p-type thermoelectricity property of GeTe by first-principles study. *J. Alloys. Compd.* **2019**, *810*, 151838. DOI
28. Feng, Y.; Li, J.; Li, Y.; et al. Band convergence and carrier-density fine-tuning as the electronic origin of high-average thermoelectric performance in Pb-doped GeTe-based alloys. *J. Mater. Chem. A.* **2020**, *8*, 11370-80. DOI
29. Li, S.; Liu, R.; Geng, Y.; et al. Electron delocalization of strontium leading to high performance in rhombohedral (Bi, Pb, Sr) co-doped GeTe thermoelectrics. *J. Mater. Chem. A.* **2026**, *14*, 39742-52. DOI
30. Perumal, S.; Bellare, P.; Shenoy, U. S.; Waghmare, U. V.; Biswas, K. Low thermal conductivity and high thermoelectric performance in Sb and Bi codoped GeTe: complementary effect of band convergence and nanostructuring. *Chem. Mater.* **2017**, *29*, 10426-35. DOI
31. Nielsen, M. D.; Ozolins, V.; Heremans, J. P. Lone pair electrons minimize lattice thermal conductivity. *Energy. Environ. Sci.* **2013**, *6*, 570-8. DOI
32. Raty, J.; Wuttig, M. The interplay between Peierls distortions and metavalent bonding in IV-VI compounds: comparing GeTe with related monochalcogenides. *J. Phys. D:. Appl. Phys.* **2020**, *53*, 234002. DOI
33. Pereira P, Sergueev I, Gorsse S, Dadda J, Müller E, Hermann RP. Lattice dynamics and structure of GeTe, SnTe and PbTe. *Physica. Status. Solidi. (b).* **2013**, *250*, 1300-7. DOI

34. Dangić, Đ.; Hellman, O.; Fahy, S.; Savić, I. The origin of the lattice thermal conductivity enhancement at the ferroelectric phase transition in GeTe. *npj. Comput. Mater.* **2021**, *7*, 523. DOI
35. Gunder, A. S.; Paillard, C.; Pandit, A.; Haleoot, R.; Bellaiche, L.; Hamad, B. Effect of the polar distortion on the thermoelectric properties of GeTe. *Eur. Phys. J. B.* **2021**, *94*, 19. DOI
36. Hong, M.; Chen, Z. G.; Yang, L.; et al. Realizing *zT* of 2.3 in $Ge_{1-x-y}Sb_xIn_y$ Te via reducing the phase-transition temperature and introducing resonant energy doping. *Adv. Mater.* **2018**, *30*, 1705942. DOI
37. Suwardi, A.; Cao, J.; Hu, L.; et al. Tailoring the phase transition temperature to achieve high-performance cubic GeTe-based thermoelectrics. *J. Mater. Chem. A.* **2020**, *8*, 18880-90. DOI
38. Li, J.; Zhang, X.; Wang, X.; et al. High-performance GeTe thermoelectrics in both rhombohedral and cubic phases. *J. Am. Chem. Soc.* **2018**, *140*, 16190-7. DOI
39. Kumar, A.; Yun, J. H.; Thoravat, S.; et al. Lattice mismatch induced lattice thermal conductivity reduction and negative thermal expansion of GeTe-based thermoelectric bulk alloys. *ACS. Appl. Mater. Interfaces.* **2025**, *17*, 45784-95. DOI
40. Xing, T.; Song, Q.; Qiu, P.; et al. High efficiency GeTe-based materials and modules for thermoelectric power generation. *Energy. Environ. Sci.* **2021**, *14*, 995-1003. DOI
41. Jin, Y.; Wang, D.; Qiu, Y.; Zhao, L. Boosting the thermoelectric performance of GeTe by manipulating the phase transition temperature via Sb doping. *J. Mater. Chem. C.* **2021**, *9*, 6484-90. DOI
42. Liu, M.; Guo, M.; Yang, Y.; et al. Tailoring the electron and phonon transport in metavalently bonded GeTe by stepwise doping. *Adv. Energy. Mater.* **2025**, *15*, 2405178. DOI
43. Suwardi, A.; Cao, J.; Zhao, Y.; et al. Achieving high thermoelectric quality factor toward high figure of merit in GeTe. *Mater. Today. Phys.* **2020**, *14*, 100239. DOI
44. D'Angelo, M.; Galassi, C.; Lecis, N. Thermoelectric materials and applications: a review. *Energies* **2023**, *16*, 6409. DOI
45. Tan, G.; Zhao, L. D.; Kanatzidis, M. G. Rationally designing high-performance bulk thermoelectric materials. *Chem. Rev.* **2016**, *116*, 12123-49. DOI PubMed
46. Zhang, M.; Gao, Z.; Lou, Q.; et al. Achieving high carrier mobility and thermal stability in plainified rhombohedral GeTe thermoelectric materials with $zT > 2$. *Adv. Funct. Mater.* **2024**, *34*, 2307864. DOI
47. Wu, D.; Feng, D.; Xu, X.; He, M.; Xu, J.; He, J. Realizing high figure of merit plateau in Ge Bi Te via enhanced Bi solution and Ge precipitation. *J. Alloys. Compd.* **2019**, *805*, 831-9. DOI
48. Mao, F.; Zhang, Z.; Zhu, S.; et al. A core-shell structure to realize high thermoelectric performance in Fe and Sb co-doped GeTe materials. *J. Materiomics.* **2026**, *12*, 101108. DOI
49. Liu, Z.; Gao, W.; Zhang, W.; Sato, N.; Guo, Q.; Mori, T. High power factor and enhanced thermoelectric performance in Sc and Bi codoped GeTe: insights into the hidden role of rhombohedral distortion degree. *Adv. Energy. Mater.* **2020**, *10*, 2002588. DOI
50. Back, S. Y.; Yun, J. H.; Cho, H.; Byeon, S.; Jin, H.; Rhyee, J. High thermoelectric performance by chemical potential tuning and lattice anharmonicity in $GeTe_{1-x}I_x$ compounds. *Inorg. Chem. Front.* **2021**, *8*, 1205-14. DOI
51. Wu, D.; Xie, L.; Chao, X.; Yang, Z.; He, J. Step-up thermoelectric performance realized in Bi_2Te_3 alloyed GeTe via carrier concentration and microstructure modulations. *ACS. Appl. Energy. Mater.* **2019**, *2*, 1616-22. DOI
52. Fan, Y.; Xie, C.; Zhang, T.; et al. Contrasting the roles of Cu interstitials and Sb substitutions in regulating ferroelectric distortions and thermoelectric properties of α-GeTe. *ACS. Appl. Energy. Mater.* **2023**, *6*, 4065-71. DOI
53. Xie, L.; Chen, Y.; Liu, R.; et al. Stacking faults modulation for scattering optimization in GeTe-based thermoelectric materials. *Nano. Energy.* **2020**, *68*, 104347. DOI
54. Chen, Y.; Li, M.; Wang, X.; et al. Copper ion diffusion by solid solution treatment advancing GeTe-based thermoelectrics. *Nat. Commun.* **2025**, *16*, 6796. DOI PubMed PMC
55. Jin, Y.; Ren, D.; Qiu, Y.; Zhao, L. Electrical and thermal transport properties of $Ge_{1-x}Pb_xCu_ySb_yTeSe_{2y}$. *Adv. Funct. Mater.* **2023**, *33*, 2304512. DOI
56. Li, M.; Xu, S.; Lyu, W.; et al. Unravelling effective-medium transport and interfacial resistance in (CaTe) (GeTe)100- thermoelectrics. *Chem. Eng. J.* **2023**, *452*, 139269. DOI
57. Duan, S.; Xue, W.; Yao, H.; et al. Achieving high thermoelectric performance by $NaSbTe_2$ alloying in GeTe for simultaneous suppression of Ge vacancies and band tailoring. *Adv. Energy. Mater.* **2022**, *12*, 2103385. DOI
58. Bu, Z.; Chen, Z.; Zhang, X.; et al. Near-room-temperature rhombohedral Ge1-Pb Te thermoelectrics. *Mater. Today. Phys.* **2020**, *15*, 100260. DOI
59. Tsai, Y.; Wei, P.; Tsou, N.; et al. Grand herringbone architecture securing the high thermoelectric performance of GeTe. *Mater. Today. Phys.* **2024**, *41*, 101329. DOI

60. Liu, M.; Sun, Y.; Zhu, J.; et al. High performance GeTe thermoelectrics enabled by lattice strain construction. *Acta. Materialia.* **2023**, *244*, 118565. DOI
61. Xu, X.; Xie, L.; Lou, Q.; Wu, D.; He, J. Boosting the thermoelectric performance of pseudo-layered $Sb_2Te_3(GeTe)_n$ via vacancy engineering. *Adv. Sci. (Weinh).* **2018**, *5*, 1801514. DOI PubMed PMC
62. Yin, L.; Liu, W.; Li, M.; et al. Interstitial Cu: an effective strategy for high carrier mobility and high thermoelectric performance in GeTe. *Adv. Funct. Mater.* **2023**, *33*, 2301750. DOI
63. Jin, Y.; Wang, D.; Zhu, Y.; et al. Contrasting roles of trivalent dopants M (M = In, Sb, Bi) in enhancing the thermoelectric performance of $Ge_{0.94}M_{0.06}Te$. *Acta. Materialia.* **2023**, *252*, 118926. DOI
64. Xiao, Y.; Wang, D.; Zhang, Y.; et al. Band sharpening and band alignment enable high quality factor to enhance thermoelectric performance in *n*-type PbS. *J. Am. Chem. Soc.* **2020**, *142*, 4051-60. DOI
65. Gao, W.; Liu, Z.; Zhang, W.; Sato, N.; Guo, Q.; Mori, T. Improved thermoelectric performance of GeTe via efficient yttrium doping. *Appl. Phys. Lett.* **2021**, *118*, 033901. DOI
66. Liu, C.; Zhang, Z.; Peng, Y.; et al. Charge transfer engineering to achieve extraordinary power generation in GeTe-based thermoelectric materials. *Sci. Adv.* **2023**, *9*, eadh0713. DOI PubMed PMC
67. Liu, D.; Wang, D.; Hong, T.; et al. Lattice plainification advances highly effective SnSe crystalline thermoelectrics. *Science* **2023**, *380*, 841. DOI
68. Ying, P.; Jian, Q.; Gong, Y.; et al. Matrix plainification leads to high thermoelectric performance in plastic Cu_2Se/SnSe composites. *Nat. Commun.* **2025**, *16*, 3305. DOI PubMed PMC
69. Bu, Z.; Li, W.; Li, J.; et al. Dilute Cu_2Te-alloying enables extraordinary performance of r-GeTe thermoelectrics. *Mater. Today. Phys.* **2019**, *9*, 100096. DOI
70. Qi, X.; Xiong, R.; Sa, B.; Zhang, X.; Li, W.; Pei, Y. Efficient rhombohedral GeTe thermoelectrics for low-grade heat recovery. *Mater. Today. Phys.* **2024**, *45*, 101466. DOI
71. Chen, H.; Song, Q.; Zhang, Z.; Wan, S.; Chen, L.; Bai, S. Anisotropic thermoelectric properties of GeTe single crystals. *J. Mater. Chem. A.* **2024**, *12*, 10974-83. DOI
72. Vankayala, R. K.; Lan, T. W.; Parajuli, P.; et al. High zT and its origin in Sb-doped GeTe single crystals. *Adv. Sci. (Weinh).* **2020**, *7*, 2002494. DOI PubMed PMC
73. Ji, D.; Haile, N. F.; Li, X.; et al. Band degeneracy and convergence in high performing thermoelectric materials. *Appl. Energy.* **2026**, *404*, 127182. DOI
74. Xing, T.; Zhu, C.; Song, Q.; et al. Ultralow lattice thermal conductivity and superhigh thermoelectric figure-of-merit in (Mg, Bi) Co-doped GeTe. *Adv. Mater.* **2021**, *33*, e2008773. DOI
75. Zhang, Q.; Ti, Z.; Zhang, Y.; et al. Ultralow lattice thermal conductivity and high thermoelectric performance in $Ge_{1-x-y}Bi_xCa_yTe$ with ultrafine ferroelectric domain structure. *ACS. Appl. Mater. Interfaces.* **2023**, *15*, 21187-97. DOI
76. Hong, M.; Wang, Y.; Feng, T.; et al. Strong phonon-phonon interactions securing extraordinary thermoelectric $Ge_{1-x}Sb_xTe$ with Zn-alloying-induced band alignment. *J. Am. Chem. Soc.* **2019**, *141*, 1742-8. DOI
77. Guo, Z.; Zhang, Q.; Wang, H.; et al. Bi-Zn codoping in GeTe synergistically enhances band convergence and phonon scattering for high thermoelectric performance. *J. Mater. Chem. A.* **2020**, *8*, 21642-8. DOI
78. Guo, Z.; Wu, G.; Yuan, M.; et al. High Thermoelectric performance and energy conversion in Hg-doped GeTe. *Adv. Funct. Mater.* **2025**, *35*, 2419431. DOI
79. Hong, M.; Wang, Y.; Liu, W.; et al. Arrays of planar vacancies in superior thermoelectric $Ge_{1-x-y}Cd_xBi_yTe$ with band convergence. *Adv. Energy. Mater.* **2018**, *8*, 1801837. DOI
80. Li, M.; Xu, S.; Hong, M.; et al. Roles of anion sites in high-performance GeTe thermoelectrics. *Adv. Funct. Mater.* **2022**, *32*, 2208579. DOI
81. Hong, M.; Zheng, K.; Lyv, W.; et al. Computer-aided design of high-efficiency GeTe-based thermoelectric devices. *Energy. Environ. Sci.* **2020**, *13*, 1856-64. DOI
82. Li, S.; Yang, Y.; Fei, X.; et al. Nanotwin architecture and ultra-high valley degeneracy lead to high thermoelectric performance in GeTe-based thermoelectric materials. *Nat. Commun.* **2026**, 17. DOI PubMed PMC
83. Feng, F.; Zhu, J.; Tan, X.; et al. Synergistic band and defect engineering realize high-efficiency CuAgSe-alloyed lead-free GeTe thermoelectrics. *Small* **2026**, *22*, e14392. DOI
84. Li, J.; Zhang, X.; Chen, Z.; et al. Low-Symmetry rhombohedral GeTe thermoelectrics. *Joule* **2018**, *2*, 976-87. DOI
85. Tan, X.; Zhang, F.; Zhu, J.; et al. High-power factor enabled by efficient manipulation interaxial angle for enhancing thermoelectrics of GeTe-Cu_2Te alloys. *ACS. Appl. Mater. Interfaces.* **2023**, *15*, 9315-23. DOI

86. Shuai, J.; Tan, X.; Guo, Q.; et al. Enhanced thermoelectric performance through crystal field engineering in transition metal-doped GeTe. *Mater. Today. Phys.* **2019**, *9*, 100094. DOI
87. Liu, Z.; Sun, J.; Mao, J.; et al. Phase-transition temperature suppression to achieve cubic GeTe and high thermoelectric performance by Bi and Mn codoping. *Proc. Natl. Acad. Sci. U. S. A.* **2018**, *115*, 5332-7. DOI PubMed PMC
88. Zheng, Z.; Su, X.; Deng, R.; et al. Rhombohedral to cubic conversion of GeTe via MnTe alloying leads to ultralow thermal conductivity, electronic band convergence, and high thermoelectric performance. *J. Am. Chem. Soc.* **2018**, *140*, 2673-86. DOI
89. Perumal, S.; Roychowdhury, S.; Negi, D. S.; Datta, R.; Biswas, K. High thermoelectric performance and enhanced mechanical stability of *p*-type $Ge_{1-x}Sb_xTe$. *Chem. Mater.* **2015**, *27*, 7171-8. DOI
90. Wu, G.; Guo, Z.; Wang, R.; et al. Structural modulation and resonant level enable high thermoelectric performance of GeTe in the mid-to-low temperature range. *J. Mater. Chem. A.* **2023**, *11*, 20497-505. DOI
91. Kim, H. S.; Gibbs, Z. M.; Tang, Y.; et al. Characterization of Lorenz number with Seebeck coefficient measurement. *APL. Mater.* **2015**, *3*, 041506. DOI
92. Srinivasan, B.; Gellé, A.; Gucci, F.; et al. Realizing a stable high thermoelectric $zT \sim 2$ over a broad temperature range in $Ge_{1-x-y}Ga_xSb_yTe$ via band engineering and hybrid flash-SPS processing. *Inorg. Chem. Front.* **2019**, *6*, 63-73. DOI
93. Zhang, C.; Yan, G.; Wang, Y.; et al. Grain boundary complexions enable a simultaneous optimization of electron and phonon transport leading to high-performance GeTe thermoelectric devices. *Adv. Energy. Mater.* **2023**, *13*, 2203361. DOI
94. Liang, R.; Yan, G.; Geng, Y.; et al. Compromise design of resonant levels in GeTe-based alloys with enhanced thermoelectric performance. *Adv. Funct. Mater.* **2024**, *34*, 2404021. DOI
95. Kumar, A.; Bhumla, P.; Kosonowski, A.; et al. Synergistic effect of work function and acoustic impedance mismatch for improved thermoelectric performance in GeTe-WC composite. *ACS. Appl. Mater. Interfaces.* **2022**, *14*, 44527-38. DOI PubMed PMC
96. Jiang, Y.; Su, B.; Yu, J.; et al. Exceptional figure of merit achieved in boron-dispersed GeTe-based thermoelectric composites. *Nat. Commun.* **2024**, *15*, 5915. DOI PubMed PMC
97. Zhu, C.; Wang, J.; Zhu, X.; et al. Effects of magnetism and size of nano-oxide inclusions on the thermoelectric properties of $Ge_{0.96}Bi_{0.06}Te$. *J. Mater. Chem. A.* **2023**, *11*, 1268-80. DOI
98. Xu, F.; Liu, B.; Ang, R. Advancing thermoelectrics in lead-free rhombohedral GeTe via interfacial engineering with MXene. *Adv. Energy. Mater.* **2025**, *15*, 2405554. DOI
99. Jin, Y.; Wang, D.; Hong, T.; et al. Outstanding CdSe with multiple functions leads to high performance of GeTe thermoelectrics. *Adv. Energy. Mater.* **2022**, *12*, 2103779. DOI
100. Wu, C.; Shi, X. L.; Wang, L.; et al. Defect engineering advances thermoelectric materials. *ACS. Nano.* **2024**, *18*, 31660-712. DOI
101. Roychowdhury, S.; Samanta, M.; Perumal, S.; Biswas, K. Germanium chalcogenide thermoelectrics: electronic structure modulation and low lattice thermal conductivity. *Chem. Mater.* **2018**, *30*, 5799-813. DOI
102. Biswas, K.; He, J.; Blum, I. D.; et al. High-performance bulk thermoelectrics with all-scale hierarchical architectures. *Nature* **2012**, *489*, 414-8. DOI
103. Wu, G.; Cai, J.; Chen, L.; et al. Defect engineering realizes superior thermoelectric performance of GeTe. *Adv. Funct. Mater.* **2024**, *34*, 2407818. DOI
104. Acharyya, P.; Roychowdhury, S.; Samanta, M.; Biswas, K. Ultralow thermal conductivity, enhanced mechanical stability, and high thermoelectric performance in $(GeTe)_{1-2x}(SnSe)_x(SnS)_x$. *J. Am. Chem. Soc.* **2020**, *142*, 20502-8. DOI
105. Jiang, Y.; Dong, J.; Zhuang, H. L.; et al. Evolution of defect structures leading to high ZT in GeTe-based thermoelectric materials. *Nat. Commun.* **2022**, *13*, 6087. DOI PubMed PMC
106. Yu, Y.; Xu, X.; Wang, Y.; et al. Tunable quantum gaps to decouple carrier and phonon transport leading to high-performance thermoelectrics. *Nat. Commun.* **2022**, *13*, 5612. DOI PubMed PMC
107. Huang, S.; Wang, C.; Yang, X.; et al. Hierarchical architectures boosting thermoelectric performance in GeTe with Sb_2Te_3 precipitates. *Adv. Funct. Mater.* **2026**, *36*, e76406. DOI
108. Wu, D.; Zhao, L. D.; Zheng, F.; Jin, L.; Kanatzidis, M. G.; He, J. Understanding nanostructuring processes in thermoelectrics and their effects on lattice thermal conductivity. *Adv. Mater.* **2016**, *28*, 2737-43. DOI
109. Li, H.; Chen, C.; Cheng, J.; et al. Lead-free GeTe alloys with high thermoelectric performance for low-grade waste heat energy harvesting. *Nano. Energy.* **2025**, *136*, 110690. DOI
110. Sarkar, D.; Das, S.; Taneja, V.; et al. Glassy thermal transport triggers ultra-high thermoelectric performance in GeTe. *Adv. Mater.* **2025**, *37*, e2417561. DOI
111. Sarkar, D.; Samanta, M.; Ghosh, T.; et al. All-scale hierarchical nanostructures and superior valence band convergence lead to ultra-high thermoelectric performance in cubic GeTe. *Energy. Environ. Sci.* **2022**, *15*, 4625-35. DOI

112. Gelbstein, Y.; Davidow, J.; Girard, S. N.; Chung, D. Y.; Kanatzidis, M. Controlling metallurgical phase separation reactions of the $Ge_{0.87}Pb_{0.13}Te$ alloy for high thermoelectric performance. *Adv. Energy. Mater.* **2013**, *3*, 815-20. DOI
113. Xie, L.; Liu, R.; Zhu, C.; et al. Enhanced thermoelectric performance in $Ge_{0.955-x}Sb_xTe/FeGe_2$ composites enabled by hierarchical defects. *Small* **2021**, *17*, e2100915. DOI
114. Zhang, Z.; Mao, F.; Yao, M.; et al. Synergistic shallow impurity levels and multiscale defect engineering in GeTe-based thermoelectrics. *J. Adv. Ceram.* **2026**, *15*, 9221258. DOI
115. Zhang, Q.; Ti, Z.; Zhu, Y.; et al. Achieving ultralow lattice thermal conductivity and high thermoelectric performance in GeTe alloys via introducing Cu_2Te nanocrystals and resonant level doping. *ACS. Nano.* **2021**, *15*, 19345-56. DOI
116. Lee, H. S.; Kim, B.; Cho, C.; et al. Herringbone structure in GeTe-based thermoelectric materials. *Acta. Materialia.* **2015**, *91*, 83-90. DOI
117. Wu, D.; Xie, L.; Xu, X.; He, J. High thermoelectric performance achieved in $GeTeBi_2Te_3$ pseudo-binary via van der Waals gap-induced hierarchical ferroelectric domain structure. *Adv. Funct. Mater.* **2019**, *29*, 1806613. DOI
118. Dangić, Đ.; Murray, ÉD.; Fahy, S.; Savić, I. Structural and thermal transport properties of ferroelectric domain walls in GeTe from first principles. *Phys. Rev. B.* **2020**, 101. DOI
119. Zhu, J.; Li, R.; Tan, X.; et al. Synergistic optimization of electronic and thermal properties in single-stage GeTe thermoelectric devices. *J. Am. Chem. Soc.* **2025**, *147*, 37555-64. DOI
120. Schwarzmüller, S.; Yang, F.; Oeckler, O. Structures and transport properties of metastable solid solutions $(NaSbTe_2)_{1-x}(GeTe)_x$. *J. Alloy. Compd.* **2019**, *806*, 774-9. DOI
121. Zhu, J.; Zhong, Y.; Tian, M.; et al. Multi-scale lattice strain engineering enables reduced deformation potential and high thermoelectric performance in GeTe alloys. *Adv. Energy. Mater.* **2026**, *16*, e71495. DOI
122. Banik, A.; Biswas, K. Synthetic nanosheets of natural van der Waals heterostructures. *Angew. Chem. Int. Ed. Engl.* **2017**, *56*, 14561-6. DOI
123. Li, Y.; Zhang, Q.; Ti, Z.; et al. Modular nanostructures advance highly effective GeTe thermoelectrics. *Acta. Materialia.* **2025**, *288*, 120883. DOI
124. Tsai, Y.; Ho, M.; Wei, P.; Wu, H. Hierarchical twinning and light impurity doping enable high-performance GeTe thermoelectrics. *Acta. Materialia.* **2022**, *222*, 117406. DOI
125. Chen, B.; Wang, K.; Wu, H. Localized crystal imperfections coupled with phase diagram engineering yield high-performance rhombohedral GeTe thermoelectrics. *Mater. Today. Phys.* **2022**, *22*, 100617. DOI
126. Bayikadi, K. S.; Wu, C. T.; Chen, L.; Chen, K.; Chou, F.; Sankar, R. Synergistic optimization of thermoelectric performance of Sb doped GeTe with a strained domain and domain boundaries. *J. Mater. Chem. A.* **2020**, *8*, 5332-41. DOI
127. Xie, L.; Yin, L.; Yu, Y.; et al. Screening strategy for developing thermoelectric interface materials. *Science* **2023**, *382*, 921-8. DOI
128. Cao, T.; Shi, X.; Li, M.; et al. Advances in bismuth-telluride-based thermoelectric devices: progress and challenges. *eScience* **2023**, *3*, 100122. DOI
129. Hu, M.; Li, M.; Wang, D.; et al. Revisiting cobalt dopability in GeTe system to design modulation-doped thermoelectrics. *Adv. Funct. Mater.* **2025**, *35*, 2421837. DOI
130. Bu, Z.; Zhang, X.; Shan, B.; et al. Realizing a 14% single-leg thermoelectric efficiency in GeTe alloys. *Sci. Adv.* **2021**, 7. DOI PubMed PMC
131. Pei, J.; Shi, J.; Li, H.; et al. Design and fabrication of segmented $GeTe/(Bi,Sb)_2Te_3$ thermoelectric module with enhanced conversion efficiency. *Adv. Funct. Mater.* **2023**, *33*, 2214771. DOI
132. Geng, Y.; He, H.; Liang, R.; et al. One-step-sintered $GeTe\text{-}Bi_2Te_3$ segmented thermoelectric legs with robust interface-connection performance. *Adv. Energy. Mater.* **2024**, *14*, 2402479. DOI
133. Xu, K.; Fu, Y.; Zuo, W.; et al. Phase-stabilized GeTe with optimized interfaces for high-performance thermoelectric energy conversion. *Energy. Environ. Sci.* **2025**, *18*, 9274-86. DOI
134. Liu, X.; Li, P.; Jiang, B.; et al. Negative enthalpy delivers thermodynamically stable and high-performance GeTe thermoelectrics. *Joule* **2026**, *10*, 102490. DOI
135. Dong, J.; Jiang, Y.; Liu, J.; et al. High thermoelectric performance in GeTe with compositional insensitivity. *Nano. Energy.* **2022**, *103*, 107809. DOI
136. Zhu, J.; Zhang, F.; Tai, Y.; et al. Enhanced thermoelectric performance and mechanical strength in GeTe enable power generation and cooling. *InfoMat* **2024**, *6*, e12514. DOI
137. Cao, J.; Tan, X. Y.; Jia, N.; et al. Designing good compatibility factor in segmented $Bi_{0.5}Sb_{1.5}Te_3$ - GeTe thermoelectrics for high power conversion efficiency. *Nano. Energy.* **2022**, *96*, 107147. DOI

138. Xu, C.; Liang, Z.; Ren, W.; Song, S.; Zhang, F.; Ren, Z. Realizing high energy conversion efficiency in a novel segmented-$Mg_3(Sb, Bi)_2$/Cubic-GeTe thermoelectric module for power generation. *Adv. Energy. Mater.* **2022**, *12*, 2202392. DOI
139. Xie, L.; Ming, C.; Song, Q.; et al. Lead-free and scalable GeTe-based thermoelectric module with an efficiency of 12. *Sci. Adv.* **2023**, *9*, eadg7919. DOI PubMed PMC
140. Guo, Z.; Song, K.; Wang, R.; et al. A high-efficiency GeTe-based thermoelectric module for low-grade heat recovery. *J. Mater. Chem. A.* **2022**, *10*, 7677-83. DOI
141. Zhang, F.; Ma, B.; Luo, Y.; et al. Promoted thermoelectric performance in cubic-phase GeTe *via* grain-boundary phase elimination under phase diagram guidance. *Energy. Environ. Sci.* **2024**, *17*, 8691-701. DOI
142. Qiu, P.; Deng, T.; Chen, L.; Shi, X. Plastic inorganic thermoelectric materials. *Joule* **2024**, *8*, 622-34. DOI
143. Samanta, M.; Biswas, K. Low thermal conductivity and high thermoelectric performance in $(GeTe)_{1-2x}(GeSe)_x(GeS)_x$: competition between solid solution and phase separation. *J. Am. Chem. Soc.* **2017**, *139*, 9382-91. DOI PubMed
144. Zhu, J.; Li, R.; Tan, X.; et al. Valence band modification and enhanced phonon-phonon interactions for high thermoelectric performance in GeTe. *Adv. Funct. Materials.* **2025**, *35*, 2417260. DOI
145. Zhu, J.; Tan, X.; Pan, D.; et al. Functionally separated electronic band engineering via multi-element doping plus high-density defects advances board-temperature-range thermoelectric performance in GeTe. *Chem. Eng. J.* **2024**, *480*, 148135. DOI
146. Suwardi, A.; Lim, S. H.; Zheng, Y.; et al. Effective enhancement of thermoelectric and mechanical properties of germanium telluride via rhenium-doping. *J. Mater. Chem. C.* **2020**, *8*, 16940-8. DOI
147. Wang, L.; Li, J.; Xie, Y.; et al. Tailoring the chemical bonding of GeTe-based alloys by MgB_2 alloying to simultaneously enhance their mechanical and thermoelectric performance. *Mater. Today. Phys.* **2021**, *16*, 100308. DOI
148. Zhi, S.; Li, J.; Hu, L.; et al. Medium entropy-enabled high performance cubic GeTe thermoelectrics. *Adv. Sci. (Weinh).* **2021**, *8*, 2100220. DOI PubMed PMC
149. Ma, B.; Ren, H.; Zhang, F.; et al. All cubic-phase δ-TAGS thermoelectrics over the entire mid-temperature range. *Small* **2023**, *19*, e2206439. DOI
150. Qiu, Y.; Jin, Y.; Wang, D.; et al. Realizing high thermoelectric performance in GeTe through decreasing the phase transition temperature *via* entropy engineering. *J. Mater. Chem. A.* **2019**, *7*, 26393-401. DOI
151. Samanta, M.; Ghosh, T.; Arora, R.; Waghmare, U. V.; Biswas, K. Realization of both n- and p-type GeTe thermoelectrics: electronic structure modulation by $AgBiSe_2$ alloying. *J. Am. Chem. Soc.* **2019**, *141*, 19505-12. DOI
152. Guo, F.; Liu, M.; Zhu, J.; et al. Suppressing lone-pair expression endows room-temperature cubic structure and high thermoelectric performance in GeTe-based materials. *Mater. Today. Phys.* **2022**, *27*, 100780. DOI
153. Wang, D.; Liu, W.; Li, M.; et al. Hierarchical architectural structures induce high performance in n-type GeTe-based thermoelectrics. *Adv. Funct. Mater.* **2023**, *33*, 2213040. DOI
154. Yin, L.; Liu, W.; Li, M.; et al. Bipolar suppression for high performance n-type GeTe-based thermoelectrics. *Adv. Energy. Mater.* **2024**, *14*, 2400340. DOI
155. Zhang, X.; Lu, X.; Jiang, P.; Bao, X. High thermoelectric performance of non-stoichiometric and oriented GeTe thin films. *Small* **2023**, *19*, e2303710. DOI
156. Sun, X.; Hou, S.; Wu, Z.; et al. Self-doping enhancing thermoelectric properties of GeTe thin films. *Appl. Phys. Lett.* **2024**, *124*, 011601. DOI
157. Ishibe, T.; Komatsubara, Y.; Ishikawa, K.; et al. Boosting thermoelectric performance in epitaxial GeTe film/Si by domain engineering and point defect control. *ACS. Appl. Mater. Interfaces.* **2023**, *15*, 26104-10. DOI
158. Abbas, S.; Jarwal, B.; Ho, T.; et al. Synergistic effect of indium doping on thermoelectric performance of cubic GeTe-based thin films. *Mater. Today. Phys.* **2024**, *49*, 101581. DOI
159. Lan, R.; Otoo, S. L.; Yuan, P.; Wang, P.; Yuan, Y.; Jiang, X. Thermoelectric properties of Sn doped GeTe thin films. *Appl. Surf. Sci.* **2020**, *507*, 145025. DOI
160. Srinivasan, B.; Le, Tonquesse. S.; Gellé, A.; et al. Screening of transition (Y, Zr, Hf, V, Nb, Mo, and Ru) and rare-earth (La and Pr) elements as potential effective dopants for thermoelectric GeTe - an experimental and theoretical appraisal. *J. Mater. Chem. A.* **2020**, *8*, 19805-21. DOI
161. Ning, S.; Zhang, Z.; Hu, X.; et al. Versatile roles of elemental doping in the optimization of the thermoelectric performance of R-GeTe studied by first principles calculations. *J. Mater. Chem. A.* **2026**, *14*, 10065-78. DOI
162. Fu, C. L.; Cheng, M.; Hung, N. T.; et al. AI-driven defect engineering for advanced thermoelectric materials. *Adv. Mater.* **2025**, *37*, e2505642. DOI PubMed PMC
163. Li, W.; Liu, M. Interpretable machine learning workflow for evaluating and analyzing the performance of high-entropy GeTe-based thermoelectric materials. *ACS. Appl. Electron. Mater.* **2023**, *5*, 4523-33. DOI

164. Perumal, S.; Roychowdhury, S.; Biswas, K. Reduction of thermal conductivity through nanostructuring enhances the thermoelectric figure of merit in $Ge_{1-x}Bi_x$ Te. *Inorg. Chem. Front.* **2016**, *3*, 125-32. DOI

165. Yue, L.; Fang, T.; Zheng, S.; et al. Cu/Sb codoping for tuning carrier concentration and thermoelectric performance of GeTe-based alloys with ultralow lattice thermal conductivity. *ACS. Appl. Energy. Mater.* **2019**, *2*, 2596-603. DOI

166. Sun, Q.; Li, M.; Shi, X.; et al. Versatile vanadium doping induces high thermoelectric performance in GeTe via band alignment and structural modulation. *Adv. Energy. Mater.* **2021**, *11*, 2100544. DOI

167. Liu, X.; Wang, W.; Wang, Y.; et al. Realizing high thermoelectric performance in GeTe-based supersaturated solid solutions. *Adv. Energy. Mater.* **2024**, *14*, 2304029. DOI

Disclaimer/Publisher's Note: All statements, opinions, and data contained in this publication are solely those of the individual author(s) and contributor(s) and do not necessarily reflect those of OAE and/or the editor(s). OAE and/or the editor(s) disclaim any responsibility for harm to persons or property resulting from the use of any ideas, methods, instructions, or products mentioned in the content.

© The Author(s) 2026. Open Access This article is licensed under a Creative Commons Attribution 4.0 International License (https://creativecommons.org/licenses/by/4.0/), which permits unrestricted use, sharing, adaptation, distribution and reproduction in any medium or format, for any purpose, even commercially, as long as you give appropriate credit to the original author(s) and the source, provide a link to the Creative Commons license, and indicate if changes were made.